



Water Resources Research



RESEARCH ARTICLE

10.1029/2022WR034186

Key Points:

- A new unsaturated hydraulic conductivity model was developed in terms of independent θ and ψ values
- Best fitting values of two parameters in the new unsaturated hydraulic conductivity model were determined from 150 soils in the calibration data set
- The new model provided reliable estimates of hydraulic conductivity for 72 soils from two independent data sets

Supporting Information:

Supporting Information may be found in the online version of this article.

Correspondence to:

J. Heitman, jlheitma@ncsu.edu

Citation:

Fu, Y., Horton, R., Ren, T., & Heitman, J. (2023). An unsaturated hydraulic conductivity model based on the capillary bundle model, the Brooks-Corey model and Waxman-Smits model. Water Resources Research, 59, e2022WR034186. https://doi.org/10.1029/2022WR034186

Received 23 NOV 2022 Accepted 17 MAY 2023

© 2023. The Authors.

This is an open access article under the terms of the Creative Commons Attribution-NonCommercial-NoDerivs License, which permits use and distribution in any medium, provided the original work is properly cited, the use is non-commercial and no modifications or adaptations are made.

An Unsaturated Hydraulic Conductivity Model Based on the Capillary Bundle Model, the Brooks-Corey Model and Waxman-Smits Model

Yongwei Fu¹, Robert Horton², Tusheng Ren³, and Joshua Heitman¹

¹Department of Crop & Soil Sciences, North Carolina State University, Raleigh, NC, USA, ²Department of Agronomy, Iowa State University, Ames, IA, USA, ³College of Land Science and Technology, China Agricultural University, Beijing, China

Abstract Soil unsaturated hydraulic conductivity (K), which depends on water content (θ) and matric potential (ψ) , exhibits a high degree of variability at the field scale. Here we first develop a theoretical hydraulic-electrical conductivity (σ) relationship under low and high salinity cases based on the capillary bundle model and Waxman and Smits model which can account for the non-linear behavior of σ at low salinities. Then the K- σ relationship is converted into a $K(\theta, \psi)$ model using the Brooks-Corey model. The model includes two parameters c and γ . Parameter c accounts for the variation of the term $(\lambda + 2)/(\lambda + 4)$ where λ is the pore size distribution parameter in the Brooks-Corey model, and the term m-n where m and nare Archie's saturation and cementation exponents, respectively. Parameter γ is the sum of the tortuosity factor accounting for the differences between hydraulic and electrical tortuosity and Archie's saturation exponent. Based on a calibration data set of 150 soils selected from the UNSODA database, the best fitting log(c) and γ values were determined as -2.53 and 1.92, -4.39 and -0.14, -5.01 and -1.34, and -5.79 and -2.27 for four textural groups. The estimated $\log_{10}(K)$ values with the new $K(\theta, \psi)$ model compared well to the measured values from an independent data set of 49 soils selected from the UNSODA database, with mean error (ME), relative error (RE), root mean square error (RMSE) and coefficient of determination (R^2) values of 0.02, 8.8%, 0.80 and 0.73, respectively. A second test of the new $K(\theta, \psi)$ model using a data set representing 23 soils reported in the literature also showed good agreement between estimated and measured $\log_{10}(K)$ values with ME of -0.01, RE of 9.5%, RMSE of 0.77 and R^2 of 0.85. The new $K(\theta, \psi)$ model outperformed the Mualem-van Genuchten model and two recently published pedo-transfer functions. The new $K(\theta, \psi)$ model can be applied for estimating K under field conditions and for hydrologic modeling without need for soil water retention curve data fitting to derive a K function.

1. Introduction

Soil hydraulic properties are essential for a variety of applications including modeling and estimation of vadose zone hydrology, groundwater flow and solute transport, and monitoring and prediction of contaminant transport and aquifer recharge (Jury & Horton, 2004; Tindall et al., 1999). Soil unsaturated hydraulic conductivity (K), which is a function of matric potential (ψ) and volumetric water content (θ), varies by orders of magnitude over relatively small spatial scales due to variations in soil properties such as soil texture and density (Assouline, 2006). Under field conditions, K also varies temporally as θ and matric potential (ψ) change. Such variability in K, therefore, requires the characterization of the $K(\theta, \psi)$ curves for unsaturated zone soils.

In general, K can be measured with steady state methods (Ankeny et al., 1991; Cui et al., 2008; Fujimaki & Inoue, 2003; Meerdink et al., 1996) or transient methods (Durner & Iden, 2011; Eching et al., 1994; Kool & Parker, 1987; van Dam et al., 1994; Wildenschild et al., 1997). Many of the methods for measuring K, either in the laboratory or in the field, are time consuming, difficult to perform accurately, and only provide local measurements on limited sampling sites, while the unsaturated zone is usually heterogeneous (Haverkamp et al., 1998). To be applicable in modeling processes, a continuous and smooth form of K function is required and thus several analytical $K(\theta)$ or $K(\psi)$ expressions have consequently been proposed (Assouline, 2001; Campbell, 1974; Kosugi, 1999; Mualem, 1976, 1978; van Genuchten, 1980). To use these models, their parameters are generally obtained by fitting the models to discrete data sets or estimating from other soils properties using pedo-transfer functions (PTFs) from more readily available soil properties such as soil texture, bulk density, and/or organic matter content (OM) (Børgesen et al., 2008; Schaap & Leij, 1998; Schaap et al., 2001; Vereecken, 1995; Vereecken et al., 1990;

FU ET AL. 1 of 25

19447973, 2023, 6, Downloa

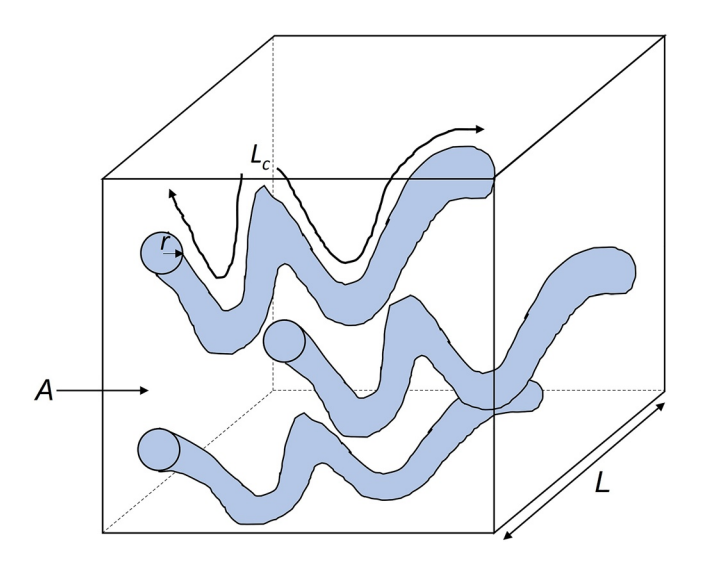


Figure 1. Schematic diagram of a soil comprised of bundle of capillary tubes (after Pfannkuch (1972) and Jackson (2008)).

Weynants et al., 2009; Wösten et al., 1999). The reliability of PTF estimates, however, depends heavily on the data set used for their development (Vereecken et al., 2010).

Both fluid flow and electrical current transmission are governed by similar macroscopic laws (i.e., Hagen-Poiseuille's law and Ohm's law) that describe the proportionality between a driving force and the resulting flow. Rooted on these similarities, there has been considerable practical interest in the relationship between K (or permeability, k) and soil electrical conductivity (σ) for rocks, soils, catalysts, ceramic filters, and concrete. Various models based on critical path analysis (Banavar & Johnson, 1987; David, 1993; Friedman & Seaton, 1998; Ghanbarian, 2020; Ghanbarian et al., 2016, 2017; Katz & Thompson, 1986; Skaggs, 2011), effective medium theory (David et al., 1990; Doyen, 1988), and bundles of capillary tubes (Mualem & Friedman, 1991) have been developed to relate K (or k) with σ . Investigators have attempted to estimate the K of unsaturated soils from σ measurements (Doussan & Ruy, 2009; Niu et al., 2015). However, joint measurements of soil hydraulic and electrical properties are scarce. As θ is one of the key contributors to soil σ (Robinson et al., 2008), it may ease of use if one can convert the K- σ relationship into $K(\theta)$ functions using the electrical conductivity models describing the σ - θ relationships.

Thus, the main objective of this study is to develop and test a new K model by integrating the capillary bundle model, the Brooks and Corey (1964) model and Waxman and Smits model. To calibrate the new K model, we selected data from the UNSODA database (Nemes et al., 2001) representing 150 soils with various textures. The calibration produced the best fitting values of the two model fitting parameters for four designated textural groupings. K values representing another 49 soils in the UNSODA database and 23 additional soils from the literature were used to test the new K model. In addition, we compared the performance of the new $K(\theta, \psi)$ model to the performance of the Mualem-van Genuchten (MVG) model and two extensively used PTFs.

2. Model Development

2.1. Capillary Bundle Model of Hydraulic and Electrical Conductivity for Soils

In this study, we assume a soil that can be represented as a bundle of capillary tubes with length l and area A (Figure 1). All capillary tubes have the same orientation, and there are no intersections between them. The schematic diagram of this soil can be found in Jackson (2008). We also assume that the pore radii (r) are assigned from a given pore size distribution (f(r)) and the pore length (l_c) is fixed, an assumption common to other studies (Banavar & Johnson, 1987; Friedman & Seaton, 1998; Le Doussal, 1989; Skaggs, 2011). The conductance in each pore is one-dimensional and parallel to the direction of the capillary axis.

According to the Hagen-Poiseuille equation for viscous laminar flow, the hydraulic conductance g_c^h of each cylindrical tube is described as,

$$g_{\rm c}^{\rm h} = \frac{\pi r^4}{8\mu l_{\rm c}} \tag{1}$$

where μ is the dynamic viscosity of water (1.0016 × 10⁻³ N s m⁻²).

As the soil consists of a bundle of capillary tubes with variable cross-sectional area (πr^2) , the total hydraulic conductance (g_t^h) of the soil is a sum of the g_c^h through all the individual capillary tubes. Integrating Equation 1 over all capillary tubes yields,

$$g_{\rm t}^{\rm h} = \frac{\pi \int_{r_{\rm min}}^{r_{\rm max}} r^4 f(r) dr}{8\mu I_{\rm c}} \tag{2}$$

where r_{\min} and r_{\max} represent the lower and upper bounds of pore radius associated with capillary pressure in the context of the capillary bundle model.

FU ET AL. 2 of 25

Thus, the permeability k (m²) of the soil is,

$$k = g_t^h \frac{\mu l}{A} = \frac{\pi \int_{r_{\min}}^{r_{\max}} r^4 f(r) dr}{8\tau A}$$
 (3)

where $\tau = l_c/l$ is the tortuosity of the capillary tubes ($\tau \ge 1$).

The transfer of electrical current in each cylindrical tube obeys Ohm's law. The electrical conductance (g_c^e) of each cylindrical pore depends on the ionic conductance in the pore water (g_{pore}^c) and the surface conductance from the adsorbed ions within the electrical double layer ($g_{surface}^c$) (Banavar & Johnson, 1987),

$$g_{\rm c}^{\rm e} = g_{\rm c}^{\rm pore} + g_{\rm c}^{\rm surface} = \frac{\pi \sigma_{\rm w} r^2}{l_{\rm c}} + \frac{2\pi \Sigma_{\rm s} r}{l_{\rm c}}$$

$$\tag{4}$$

where σ_w is the electrical conductivity of the water occupying the cylindrical tube and Σ_s is the specific surface conductance representing the "anomalous" conduction in the electrical double layer (Revil & Glover, 1998).

2.2. $k(\theta, \psi)$ Model for Soils With Negligible Surface Conduction

In the following, we will first consider clay-free soils or soils with high salinity where electrical conduction occurs predominantly via pore space rather than surface area. Under this condition, surface conduction is negligible (i.e., $\Sigma_s \approx 0$) thus only the first term in Equation 4 is kept and used in the following derivation. Then an analog expression of Equation 3 can be derived for the electrical conductivity σ (S m⁻¹) of the soil as,

$$\sigma = \frac{\pi \sigma_{\rm w} \int_{r_{\rm min}}^{r_{\rm max}} r^2 f(r) dr}{\tau A} \tag{5}$$

Substituting τA in Equation 5 into Equation 3, a k- σ relationship is obtained,

$$k = \frac{1}{8} \frac{\int_{r_{\min}}^{r_{\max}} r^4 f(r) dr}{\int_{r_{\min}}^{r_{\max}} r^2 f(r) dr} \frac{\sigma}{\sigma_w}$$
 (6)

which is equivalent to

$$k = \frac{1}{8} \frac{\int_{\psi_{\min}}^{\psi_{\max}} \left(\frac{1.49 \times 10^{-5}}{\psi}\right)^4 f(r) dr}{\int_{\psi_{\min}}^{\psi_{\max}} \left(\frac{1.49 \times 10^{-5}}{\psi}\right)^2 f(r) dr} \frac{\sigma}{\sigma_w}$$
(7)

with $r \approx 1.49 \times 10^{-5} / |\psi|$ at 20°C by the Young-Laplace equation if ψ is expressed in unit of m of H_2O and the contact angle of water on the solid phase is assumed to be 0 (Jury & Horton, 2004), and ψ_{max} and ψ_{min} are the matric potentials corresponding to r_{max} and r_{min} .

The term f(r)dr in Equation 7 represents the contribution to θ of the water-filled pores with radii between r and r + dr (Mualem, 1976), which can be expressed as,

$$d\theta = f(r)dr \tag{8}$$

Inserting Equation 8 into Equation 7 gives,

$$k = \frac{\left(1.49 \times 10^{-5}\right)^2}{8} \frac{\int_{\nu_{\min}}^{\nu_{\max}} \frac{1}{\nu^4} d\theta}{\int_{\nu_{\min}}^{\nu_{\max}} \frac{1}{\nu^2} d\theta} \frac{\sigma}{\sigma_w}$$
(9)

A correspondence between a real soil and the capillary bundle model can be established by using the soil water retention curve (SWRC) (i.e., the ψ and θ relationship). Here we use the Brooks and Corey (1964) model,

$$S_{\rm e} = \frac{\theta - \theta_{\rm r}}{\theta_{\rm s} - \theta_{\rm r}} = \left(\frac{\psi_{\rm b}}{\psi}\right)^{\lambda} \quad \text{for } \psi < \psi_{\rm b}$$
 (10a)

FU ET AL. 3 of 25

$$S_{\rm e} = 1 \quad \text{for } \psi < \psi_{\rm b} < 0 \tag{10b}$$

where $S_{\rm e}$ is effective saturation, $\theta_{\rm s}$ and $\theta_{\rm r}$ are the saturated and residual water contents, respectively; λ (>0) is a shape parameter related to pore size distribution, and $\psi_{\rm b}$ is the air-entry pressure at which the saturated soil starts to drain and air begins to replace water in the void spaces. In practice, $\psi_{\rm b}$ is associated with the $r_{\rm max}$ ($\psi_{\rm max}$) since it defines the threshold at which the largest pores begin to drain. When $\psi = \psi_{\rm min}$, the soil reaches the residual moisture condition and $\theta = \theta_{\rm r}$.

The first-order derivative of Equation 10 is,

$$\frac{d\theta}{dw} = (\theta_{\rm r} - \theta_{\rm s})\lambda(\psi_{\rm b})^{\lambda}\psi^{(-\lambda - 1)} \tag{11}$$

For values of $\psi \ge \psi_b$, the soil pores are completely filled with water, if macropore flow near saturation is ignored, the soil permeability can be considered approximately equal to the saturated permeability (k_{sat}) . The following k- σ relationship for the saturated soil is obtained by combining Equations 9 and 11,

$$k_{\text{sat}} = \frac{\left(1.49 \times 10^{-5}\right)^2}{8} \frac{\lambda + 2}{\lambda + 4} \frac{\left[\psi^{\lambda + 2}\right]_{\psi_{\text{min}}}^{\psi_{\text{b}}}}{\left[\psi^{\lambda + 4}\right]_{\psi_{\text{min}}}^{\psi_{\text{b}}}} \frac{\sigma_{\text{sat}}}{\sigma_w} = \frac{\left(1.49 \times 10^{-5}\right)^2}{8} \frac{\lambda + 2}{\lambda + 4} \frac{1}{\psi_b^2} \frac{\sigma_{\text{sat}}}{\sigma_w}$$
(12)

where σ_{sat} is the electrical conductivity of fully saturated soil. Interestingly, if we recast Equation 12 with the Young-Laplace equation, it becomes

$$k_{\text{sat}} = \frac{1}{8} \left(\sqrt{\frac{\lambda + 2}{\lambda + 4}} r_{\text{max}} \right)^2 \frac{\sigma_{\text{sat}}}{\sigma_w}$$
 (13)

Equation 13 is similar in form to the k- σ relationship introduced by Friedman and Seaton (1998) (i.e., $k_{\text{sat}} = (1/8) \times r_{\text{c}}^{\text{sat}^2} \times (\sigma_{\text{sat}}/\sigma_{\text{w}})$ in which $r_{\text{c}}^{\text{sat}}$ is the critical pore radius for saturated soils). Friedman and Seaton (1998) related k_{sat} to σ_{sat} through their conductance of the critical pore, which is only affected by $r_{\text{c}}^{\text{sat}}$.

Johnson et al. (1986) also introduced a similar k- σ relationship in the high salinity limit as Equation 6,

$$k_{\text{sat}} = \frac{1}{8} \Lambda_{\text{sat}}^2 \frac{\sigma_{\text{sat}}}{\sigma_w} \tag{14}$$

where Λ_{sat} is the dynamic pore radius, which is defined as a weighted pore volume (V) to surface area (S) ratio weighted by the normalized potential $(\nabla\Gamma)$ in the absence of surface conduction,

$$\frac{2}{\Lambda_{\text{sat}}} = \frac{\int |\nabla \Gamma|^2 dS}{\int |\nabla \Gamma|^2 dV}$$
 (15)

For a soil comprised of capillary tubes, if we assume a weighted pore radius of this soil ($\langle r \rangle$) and constant electric field everywhere, $\Lambda_{\text{sat}} = 2V/S = 2(\pi \langle r \rangle^2 l_c)/(2\pi \langle r \rangle l_c) = \langle r \rangle$. Therefore, we identify the following equality between Equations 13 and 14 and the Friedman and Seaton (1998) relationship,

$$\Lambda_{\text{sat}} = \langle r \rangle = r_{\text{c}}^{\text{sat}} = \sqrt{\frac{\lambda + 2}{\lambda + 4}} r_{\text{max}}$$
 (16)

This equation provides an explanation for the $\sqrt{(\lambda+2)/(\lambda+4)}r_{\text{max}}$ in Equation 13 and shows a linear relationship between $\langle r \rangle$ and r_{max} under fully saturated conditions where the coefficient is related to the pore size distribution. Ghanbarian-Alavijeh and Hunt (2012), Ghanbarian et al. (2017) derived a similar expression to Equation 16, which related the critical pore radius (r_c) to r_{max} with pore-solid fractal parameters (*D*). It is not a coincidence as Le Doussal (1989) also reported that $\Lambda_{\text{sat}} \propto r_c$ in the porous media (fixed *l* and variable *r*) we describe here.

For the unsaturated soil, combining Equations 9 and 11 yields,

$$k_{\rm u} = \frac{\left(1.49 \times 10^{-5}\right)^2}{8} \frac{\lambda + 2}{\lambda + 4} \frac{\left[\psi^{\lambda + 2}\right]_{\psi_{\rm min}}^{\psi}}{\left[\psi^{\lambda + 4}\right]_{\psi_{\rm min}}^{\psi}} \frac{\sigma_{\rm u}}{\sigma_{\rm w}} = \frac{\left(1.49 \times 10^{-5}\right)^2}{8} \frac{\lambda + 2}{\lambda + 4} \frac{1}{\psi^2} \frac{\sigma_{\rm u}}{\sigma_{\rm w}}$$
(17)

FU ET AL. 4 of 25

where $k_{\rm u}$ and $\sigma_{\rm u}$ are the permeability and electrical conductivity of unsaturated soil, respectively.

An analogous expression to Equation 16 can thus be derived for unsaturated soil:

$$\Lambda_{\rm u} = r_{\rm c}^{\rm u} = \sqrt{\frac{\lambda + 2}{\lambda + 4}} r \tag{18}$$

where $r_c^{\rm u}$ and $\Lambda_{\rm u}$ are the critical radius and length scale for unsaturated soil, respectively.

Equations 16 and 18 then give $\Lambda_u = \Lambda_{sat} S_e^{1/\lambda}$. Revil et al. (2014) assumed two models for the dependence of Λ on the degree of saturation (S_w) : (1) $\Lambda_u = \Lambda_{sat} S_w$; (b) $\Lambda_u = \Lambda_{sat} S_w^n$ in which n is Archie's saturation exponent. This means both models that Revil et al. (2014) assumed can be regarded as the special cases (i.e., (a) $\theta_r = 0$ and $\lambda = 1$; (b) $\theta_r = 0$ and $\lambda = n$) of our model. It is noteworthy that Ghanbarian et al. (2017) derived a more general framework between Λ_u and Λ_{sat} , which reduces to our proposed model (i.e., $\Lambda_u = \Lambda_{sat} Se^{1/\lambda}$) when the critical water content (θ_c), β and 3-D in their model are equal to θ_r , $\theta_s - \theta_r$ and λ , respectively. Details can be found in Equations 12 and 13 in Ghanbarian et al. (2017).

To apply Equation 17 in a more general case, the electrical conductivity in these equations must be rewritten because joint measurements of hydraulic properties and electrical properties are scarce for most soils. The electrical conductivity of unsaturated soils can be defined using Waxman and Smits (1968) model:

$$\sigma_{\rm u} = \phi^m S_{\rm w}^n \left(\sigma_{\rm w} + \frac{\sigma_{\rm EDL}}{S_{\rm w}} \right) \tag{19}$$

where σ_{EDL} is the electrical conductivity of the electrical double layer (EDL) which is caused by the conduction via ions at the mineral-water interface within the EDL. Because we ignore the contribution of surface conduction, the electrical conductivity variables (i.e., σ_{sat} and σ_{u}) in Equations 12 and 17 only consider the ionic conduction through the pore space. Then Equation 19 reduces to the Archie's first and second law, and it can be expressed as:

$$\sigma_{\rm u} = \sigma_{\rm sat} S_{\rm w}^n = \sigma_{\rm w} \phi^m S_{\rm w}^n \tag{20}$$

where ϕ is porosity, and m is a cementation exponent. Friedman (2005) reviewed the m values of various porous media and reported a typical range from 1.2 to 4.0. Gorman and Kelly (1990) obtained a best fitting value of m (1.30) for Ottawa sand mixtures of various grain sizes.

Inserting Equation 20 into Equation 17 leads to

$$k_{\rm u} = \frac{\left(1.49 \times 10^{-5}\right)^2}{8} \frac{\lambda + 2}{\lambda + 4} \frac{1}{\psi^2} \phi^{m-n} \theta^n \tag{21}$$

When deriving the k and σ of the soil (Equations 3 and 5), we assume the same length of the pathways (l_c), and thus tortuosity ($\tau = l_c l l$), for water flow and electrical current. This assumption is valid only for two extreme cases: a homogenous porous media with mono-sized pores or a highly heterogeneous porous media with a broad distribution of pore size (Ghanbarian et al., 2013). In a three-dimensional random porous media, model simulation results at a microscopic level show that the pathway for water flow is more tortuous than that for electrical current at a porosity of 0.50, and that this difference is more abrupt for a lower porosity of 0.35 (X. Zhang & Knackstedt, 1995). Additionally, Martys and Garboczi (1992) report that even at high porosity, there are more stagnant areas (with little or no flow) for water flow than for electrical current. Ghanbarian et al. (2013) reviewed the tortuosity models for unsaturated porous media and reported that most of them are power functions of θ (e.g., Coleman & Vassilicos, 2008; Millington & Quirk, 1961). Thus, we add a saturation-dependent tortuosity term θ^{β} into Equation 21 to account for differences between hydraulic and electrical tortuosity,

$$k_{\rm u} = \frac{\left(1.49 \times 10^{-5}\right)^2}{8} \frac{\lambda + 2}{\lambda + 4} \frac{1}{w^2} \phi^{m-n} \theta^{n+\beta} \tag{22}$$

where β is correction factor for tortuosity.

An expression for saturated soil also can be obtained by adding ϕ^{β} into Equation 12,

FU ET AL. 5 of 25

$$k_{\text{sat}} = \frac{\left(1.49 \times 10^{-5}\right)^2}{8} \frac{\lambda + 2}{\lambda + 4} \frac{1}{\psi_h^2} \phi^{m+\beta}$$
 (23)

Dividing Equation 22 by Equation 23 gives the relative permeability k_r ,

$$k_{\rm r} = S_{\rm e}^{\frac{2}{\lambda}} S_{\rm w}^{\beta + n} \approx S_{\rm e}^{\frac{2}{\lambda} + n + \beta} \tag{24}$$

It is recognized that Archie's saturation exponent (n) is typically close to 2 (Ewing & Hunt, 2006; Friedman, 2005; Fu et al., 2021; Rhoades et al., 1976). Mualem and Friedman (1991) used a semi-empirical hydraulic conductivity model to derive n (2.5) for coarse-textured soils. If we fix n as 2, then Equation 24 reduces to the k_r function proposed by Mualem (1976) and the tortuosity factor β in Equation 24 is identical to the empirical tortuosity parameter in the Mualem-Brooks and Corey model. For the specific case of $\beta = 1$, n = 2 and $\theta_r = 0$, Equation 24 reduces to the k_r relationship in Campbell (1974).

2.3. $k(\theta, \psi)$ Model for Soil With Significant Surface Conduction

We next consider a low salinity limit at which surface conduction via electrical double layer is dominant compared to pore water conductivity ($\sigma_w/\Sigma_s \to 0$). The electrical conductance of each capillary tube thus depends on the surface conduction only. Then Equation 4 becomes,

$$g_{\rm c}^{\rm e} = g_{\rm c}^{\rm surface} = \frac{2\pi\Sigma_{\rm s}r}{l_{\rm c}} \tag{25}$$

 $\Sigma_{\rm s}$ can be related to the $\sigma_{\rm EDL}$ in each capillary tube as (see details in Equation 5.5 in O'Konski (1960)):

$$\sigma_{\rm EDL} = \frac{2\Sigma_{\rm s}}{r} \tag{26}$$

Then we obtain the electrical conductivity σ (S m⁻¹) of the soil at low salinity limit,

$$\sigma = \frac{\pi \sigma_{\text{EDL}} \int_{r_{\text{min}}}^{r_{\text{max}}} r^2 f(r) dr}{\tau A}$$
 (27)

Note that Equation 27 assumes that the electric current transported via counterions in the electrical double layer travels along the same tortuous path as the current transported via the pore electrolyte which was also assumed in the Waxman and Smits (1968) model. More discussion about this assumption can be found in Section 2.2.4.2 in Binley and Slater (2020) and Section 2.4 in Revil et al. (2018).

Combining Equations 5 and 27 yields a k- σ relationship slightly different from Equation 6,

$$k = \frac{1}{8} \frac{\int_{r_{\min}}^{r_{\max}} r^4 f(r) dr}{\int_{r_{\min}}^{r_{\max}} r^2 f(r) dr} \frac{\sigma}{\sigma_{\text{EDL}}}$$
(28)

At the same condition $(\sigma_w/\Sigma_s \to 0)$, Equation 19 reduces to,

$$\sigma_{\rm u} = \phi^m S_{\rm w}^{n-1} \sigma_{\rm EDL} \tag{29}$$

For Equation 28, surface conduction via the pore surface area is dominant. With increasing specific surface area ($\alpha 1/r$ for each capillary tube by assuming a constant particle density), $\sigma_{\rm sat}$ increases but $k_{\rm sat}$ decreases with decreasing r as $\sigma_{\rm sat}/\sigma_{\rm EDL}$ (= ϕ^m), which is defined by Glover (2009) as the connectedness of pore space, holds constant. Thus Equation 28 predicts a negative correlation between $k_{\rm sat}$ and $\sigma_{\rm sat}$ which is consistent with the findings of Purvance and Andricevic (2000).

Following the same derivation steps above, we arrive at expressions similar to Equations 22 and 23 for unsaturated and saturated soils, respectively:

$$k_{\rm u} = \frac{\left(1.49 \times 10^{-5}\right)^2}{8} \frac{\lambda + 2}{\lambda + 4} \frac{1}{\psi^2} \phi^{m-n+1} \theta^{n+\beta-1} \tag{30}$$

FU ET AL. 6 of 25

$$k_{\text{sat}} = \frac{\left(1.49 \times 10^{-5}\right)^2}{8} \frac{\lambda + 2}{\lambda + 4} \frac{1}{\psi_{\text{h}}^2} \phi^{m+\beta}$$
 (31)

Dividing Equation 30 by Equation 31 gives the relative permeability k_r ,

$$k_{\rm r} = S_{\rm e}^{\frac{2}{\lambda}} S_{\rm w}^{\beta + n - 1} \approx S_{\rm e}^{\frac{2}{\lambda} + n + \beta - 1} \tag{32}$$

Again, if we fix n as 2, Equation 32 reduces to the Burdine-Brooks-Corey model and the tortuosity factor β in Equation 32 is identical to the empirical tortuosity parameter in the Burdine (1953) model.

2.4. The General Expression of $K(\theta, \psi)$ Model for Unsaturated Soils

In the previous sections, we derive $k(\theta, \psi)$ functions at two extreme limits (high and low salinity). Both of them have a term $(\lambda + 2)/(\lambda + 4)$, which relates to the pore size distribution parameter λ . Nasta et al. (2013) summarized the statistical λ results based on 62 soils from the GRIZZLY Database (Haverkamp et al., 1997) and 197 soils from the HYPRES Database (Wösten et al., 1999). They reported average λ values of 0.43 (ranging from 0.06 to 2.59) for the GRIZZLY Database and 0.63 (ranging from 0.05 to 3.84) for the HYPRES Database, which resulted in a limited range of 0.51–0.74 for the term $(\lambda + 2)/(\lambda + 4)$.

For most soils, both ionic conduction and surface conduction contribute to the bulk electrical conduction. Thus, by unifying Equations 22 and 30, we obtain the following general expression of the $k(\theta, \psi)$ function for unsaturated soils based on the capillary bundle model, Brooks-Corey model and Waxman and Smits equation,

$$k_{\rm u} = \frac{\left(1.49 \times 10^{-5}\right)^2}{8} c \frac{1}{w^2} \theta^{\gamma} \tag{33}$$

where c is an empirical parameter that accounts for the variation of the term $(\lambda + 2)/(\lambda + 4)$, ϕ and the term m - n. γ ranges from $n + \beta - 1$ to $n + \beta$.

Then hydraulic conductivity K (m s⁻¹) is related to the permeability $k_{\rm u}$ (m²) in Equation 33 with a scale factor $\rho_{\rm w} g/\mu$ (9.77 × 10⁶ m⁻¹ s⁻¹) as,

$$K = \frac{\rho_{\rm w}g}{\mu}k_{\rm u} = 2.71 \times 10^{-4} \frac{c}{w^2}\theta^{\gamma}$$
 (34)

where ρ_w is the density of water (1 Mg m⁻³ at 20°C) and g is the local acceleration due to gravity (9.81 m s⁻²). Besides, Equation 34 predicts a relatively sharp increase in K near saturation when ψ approaches 0. Thus, we use K_{sat} as the upper limit of Equation 34 to avoid unreasonable fitted K values (i.e., $K > K_{\text{sat}}$) and impose the following constraint during the optimization,

$$K = 2.71 \times 10^{-4} \frac{c}{\psi^2} \theta^{\gamma} \quad \text{if } K < K_{\text{sat}}$$

$$K = K_{\text{sat}} \quad \text{if } K \ge K_{\text{sat}}$$
(35)

2.5. Physical Constraints of Parameters

As increasing K with decreasing θ (or ψ) is physically impossible, parameter constraints must be applied to prevent such inconsistencies. That means the $K(\theta)$ or $K(\psi)$ function must be strictly monotonic, that is, the first derivative of Equation 34 >0:

$$\frac{dK}{d\theta} \approx 2.71 \times 10^{-4} c \left(\frac{2}{\lambda} + \gamma\right) \frac{\theta^{\frac{2}{\lambda} + \gamma - 1}}{\frac{2}{\theta_s^{\lambda}} \psi_b^2} > 0 \tag{36}$$

With the condition $\theta > 0$, Equation 36 yields the general constraint for γ :

$$\gamma > -\frac{2}{\lambda} \tag{37}$$

FU ET AL. 7 of 25

It is also noteworthy that Equation 34 is only valid when $\psi < \psi_b$. When $\psi \approx \psi_b$ and $\theta \approx \theta_s$, Equation 34 provides a theoretical maximum value as $K_{\text{max}} = 2.71 \times 10^{-4} \, c(\theta_s)^{\gamma} / (\psi_b)^2$. Theoretically, K_{max} must be smaller than K_{sat} , thus parameter c is thus subject to the following upper constraint,

$$c < \frac{K_{\text{sat}}\psi_b^2}{2.71 \times 10^{-4}\theta^{\gamma}} \tag{38}$$

3. Materials and Methods

3.1. Data Sets

SWRC and unsaturated hydraulic conductivity curve (HCC) data (UNSODA version 2.0) (Nemes et al., 2001) were used to evaluate the new hydraulic conductivity model (Equation 35). For each selected soil, the data included measured values of at least seven data points for both water retention curve ($\theta(\psi)$) and HCC ($K(\psi)$). In addition, we used all the data from the database when $K(\psi)$ and $\theta(\psi)$ were available at the same ψ values or $K(\theta)$ and $\psi(\theta)$ were available at the same θ values resulting in 199 soils and about 4,000 K(θ , ψ) data points covering a wide range of texture, bulk density, organic OM and cation exchange capacity. Complete sand, silt, and clay percentages (USDA systems) were available for 104 soils. All 199 soils were grouped with their UNSODA codes, then soils with order numbers of multiplier of four were assigned as the validation data set and the remaining soils were used as the calibration data set. Thus, the 199 soils were divided into a calibration data set of 150 soils including 3,053 K(θ , ψ) data points and a validation data set (data set 1) of 49 soils including 1,018 K(θ , ψ) data points, which ensured that both the calibration and validation groups covered a wide range of matric potential values.

In addition to the UNSODA database, the new model (Equation 35) was also evaluated using another independent data set (validation data set 2) of 23 soils including 416 K(θ , ψ) data points, which was obtained from the literature (Table 1). The validation data set 2 comprised of Fontainebleau sand, Collias loam and Avignon silty clay loam (Doussan & Ruy, 2009); Oso Falco fine sand and Columbia sandy loam (Tuli & Hopmans, 2004); Gilat sandy loam, Rehovot sand, and Pachapa Fine sandy clay (Mualem, 1976); Tottori dune sand (Sakai & Toride, 2007); Guelph loam (Elrick & Bowman, 1964); Rubicon sandy loam (Topp, 1969); Rideau clay loam (Topp, 1971); Wray Dune sand (Gillham et al., 1979); Rhinluch sand (Schindler & Müller, 2006); Berlin sand (Peters, 2013); Shonai sand (Mehta et al., 1994); Fine sand, UC sandy loam, Gambarra loam, Gambarra B clay loam, Cubbaroo clay loam, Tarra clay, and Carrigan heavy clay (Minasny & Field, 2005). The water retention curves ($S(-\psi)$) and relative HCCs (($K/K_{sat}(-\psi)$)) of the 222 soils in the three data sets are presented in Figure 2.

The textural information of the 222 soils (i.e., 150 soils in the calibration data set, 49 soils in validation data set 1, and 23 soils in validation data set 2) is summarized in Figure 3. These data sets provided a wide coverage of soil types with a preponderance of sand, silt loam, loam, and sandy loam soils, along with a few clay soils. The ranges of soil properties are presented in Table 2.

3.2. Mualem-Van Genuchten Model

The reliability of the new hydraulic conductivity model (Equation 35) was evaluated using validation data set 1 and data set 2. We also compared the performance of the proposed relationship to that of the widely used MVG (van Genuchten, 1980) model. The MVG model is given as follows,

$$K = K_0 S_e^q \left\{ 1 - \left[1 - S_e^{[p/(p-1)]} \right]^{(1-1/p)} \right\}^2$$
 (39)

where K_0 is hydraulic conductivity (m s⁻¹) acting as a matching point, q is a factor that accounts for the tortuosity and the connectivity of the soil, and p (>1) is the shape parameter of the $\theta(\psi)$ curve.

The van Genuchten (1980) model is the basis for the estimation of K with the MVG approach. Unlike the new hydraulic conductivity model, one must first fit the parameters of the van Genuchten model before using the MVG model. The model parameters can be determined by fitting the van Genuchten (1980) model to the $\theta(\psi)$ measurements. The van Genuchten (1980) model describes the $\theta(\psi)$ curve as,

$$S_{\rm e} = \frac{\theta - \theta_{\rm r}}{\theta_{\rm s} - \theta_{\rm r}} = \left[\frac{1}{1 + (\alpha |\psi|)^p} \right]^{(1 - 1/p)} \tag{40}$$

FU ET AL. 8 of 25

1944/973, 2023, 6, Downloaded from https://agupubs.onlinelibrary.wiley.com/doi/10.1029/2022WR034186 by North Carolina State Universit, Wiley Online Library on [05/06/2023]. See the Terms and Conditions (https://onlinelibrary.wiley.

Table 1Soil Name, Particle Size Distribution, Bulk Density (ρ_b), Saturated Hydraulic Conductivity (K_{sat}) and Sources of Soils Information Included in Validation Data Set 2

Information Included in Validation Data Set 2								
	Particle size distribution		stribution	$\rho_{\rm b}$ $K_{\rm sat}$				
Soil name	Sand	Silt	Clay	g cm ⁻³	m s ⁻¹	Sources		
Fontainebleau sand	1.00	0	0	1.70	3.09×10^{-4}	Doussan and Ruy (2009)		
Collias loam	0.38	0.49	0.14	1.48	1.86×10^{-5}	Doussan and Ruy (2009)		
Avignon silty clay loam	0.16	0.51	0.33	1.64	4.07×10^{-5}	Doussan and Ruy (2009)		
Oso Falco fine sand	1.00	0	0	1.56	1.31×10^{-7}	Tuli and Hopmans (2004)		
Columbia sandy loam	0.68	0.22	0.10	1.4	2.28×10^{-7}	Tuli and Hopmans (2004)		
Gilat sandy loam	-	-	-	-	2.00×10^{-6}	Mualem (1976)		
Rehovot sand	-	-	-	-	1.27×10^{-4}	Mualem (1976)		
Pachapa Fine sandy clay	-	-	-	-	1.40×10^{-6}	Mualem (1976)		
Tottori dune sand	-	-	-	-	1.14×10^{-5}	Sakai and Toride (2007)		
Guelph loam	-	-	-	1.26	3.66×10^{-6}	Elrick and Bowman (1964)		
Rubicon sandy loam	0.65	0.26	0.09	1.35	5.17×10^{-6}	Topp (1969)		
Rideau clay loam	0.36	0.29	0.35	1.28	2.31×10^{-6}	Topp (1971)		
Wray Dune sand	-	-	-	1.7	5.95×10^{-5}	Gillham et al. (1979)		
Rhinluch sand	-	-	-	-	3.80×10^{-6}	Schindler and Müller (2006)		
Berlin sand	1.00	0	0	1.55	6.23×10^{-5}	Peters (2013)		
Shonai sand	0.93	0.01	0.06	1.40	7.79×10^{-5}	Mehta et al. (1994)		
Fine sand	1.00	0	0	1.48	-	Minasny and Field (2005)		
UC sandy loam	0.74	0.09	0.17	1.63	1.60×10^{-4}	Minasny and Field (2005)		
Gambarra loam	0.51	0.35	0.14	1.67	2.19×10^{-4}	Minasny and Field (2005)		
Gambarra B clay loam	0.40	0.24	0.36	1.69	9.77×10^{-5}	Minasny and Field (2005)		
Cubbaroo clay loam	0.35	0.27	0.38	1.42	-	Minasny and Field (2005)		
Tarra clay	0.09	0.35	0.56	1.12	-	Minasny and Field (2005)		
Carrigan heavy clay	0.17	0.21	0.62	1.34	-	Minasny and Field (2005)		

where α (>0, cm⁻¹) is a scale parameter relative to the matric potential axis (van Lier & Pinheiro, 2018).

3.3. Fitting Parameters to Hydraulic Data

The parameters in Equations 10 and 40 were fitted to water retention data. The objective function that was minimized is given by,

$$O_{\mathbf{w}}(v) = \sum_{i=1}^{N_{\mathbf{w}}} \left(\theta_i - \theta_i'\right)^2 \tag{41}$$

where θ_i and θ_i' are the measured and fitted water content values, respectively, and $N_{\rm w}$ is number of measured water retention points of each soil sample. ν is the parameter vector which is $\{\theta_{\rm s}, \theta_{\rm r}, \lambda, \psi_{\rm b}\}$ for Equation 10 and $\{\theta_{\rm s}, \theta_{\rm r}, \gamma, p\}$ for Equation 40.

Equations 35 and 39 were fitted to the $K(\theta, \psi)$ measurements with a least squares method by minimizing the following objective function:

$$O_{K}(v) = \sum_{i=1}^{N_{K}} \left[\log_{10}(K_{i}) - \log_{10}(K_{i}') \right]^{2}$$
(42)

where K_i and K_i' are the measured and fitted hydraulic conductivity, respectively, N_K is the number of measured $K(\theta, \psi)$ data points and ν is the parameter vector $\{c, \gamma\}$. During optimization, the parameters c and γ are subject to the constraints $0 < c < K_{sat}\psi_b^2/2.71 \times 10^{-4}\theta_s^{\gamma}$ and $\gamma > -2/\lambda$ where ψ_b and λ are inferred from water retention

FU ET AL. 9 of 25

1944/7973, 2023, 6, Downboaded from https://agupubs.onlinelibrary.wiley.com/doi/10.1029/2022WR034186 by North Carolina State Universit, Wiley Online Library on [05/06/2023]. See the Terms and Conditions (https://onlinelibrary.wiley.

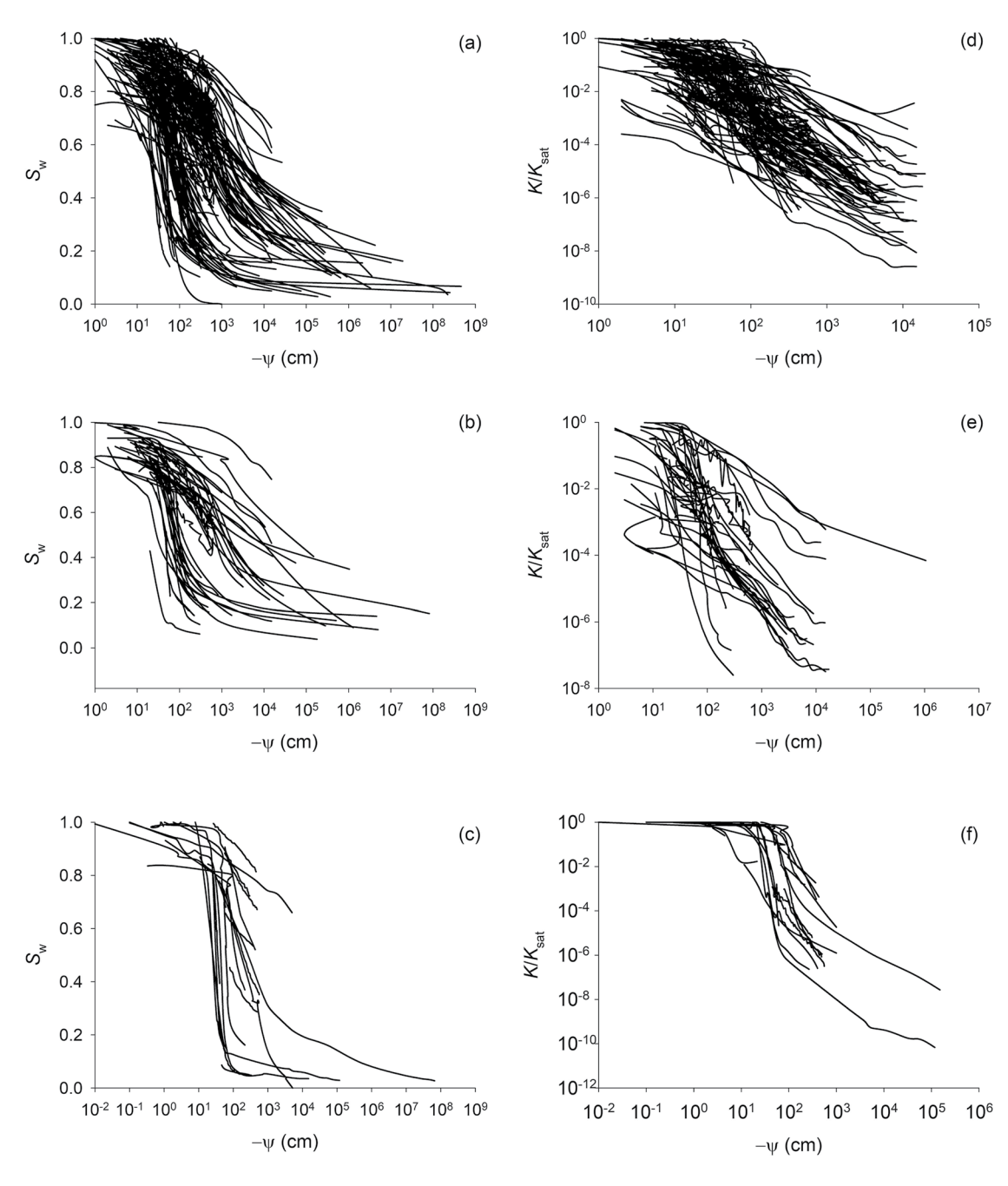


Figure 2. (a–c) Water retention curves $(S(\psi))$ for soils in the calibration, validation 1 and validation 2 data sets, respectively; (d–f) hydraulic conductivity curves $(K/K_{sat}(\psi))$ for soils in the calibration, validation 1 and validation 2 data sets, respectively.

curve measurements using Equation 10 first. Logarithmic values of K were used in Equation 42 to achieve variance homogeneity. For MVG model, we use the α and p from Equation 40 to compute S_e first then optimize K_0 and q in Equation 39. We imposed the following additional constraints recommended by Schaap and Leij (2000) during the optimization: $0 < K_0 < K_s$ and -2 - 2/(p-1) < q < 100.

Several metrics were used to evaluate the model performance: (a) the mean error (ME) describing the average bias, (b) the relative error (RE) describing the magnitude of the bias compared to the measured K values, (c) the root mean squared error (RMSE) describing the spread of the errors around the measured K values, and (d) the coefficient of determination (R^2) describing how well observed outcomes were replicated by the model. The parameters ME, RE, RMSE and R^2 were used as summary statistics for all results, and they are given by,

FU ET AL. 10 of 25

1944/973, 2023, 6, Downloaded from https://agupubs.onlinelibrary.wiley.com/doi/10.1029/2022WR034186 by North Carolina State Universit, Wiley Online Library on [05/06/2023].

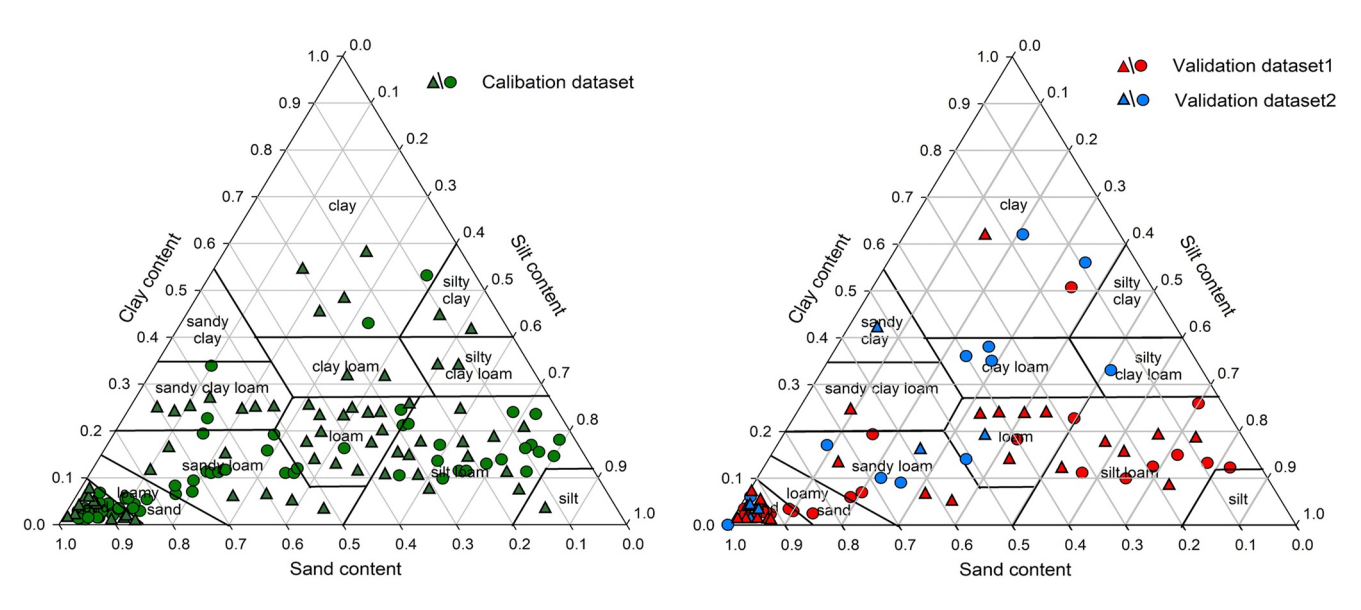


Figure 3. Texture classes of the soils used to calibrate and validate the new hydraulic conductivity model (Equation 35). Circles represent soils with complete sand, silt, and clay percentages (USDA system) whereas soils with incomplete sand, silt and clay percentages are plotted as triangles with approximate texture information.

$$ME = \frac{\sum (\log_{10} K_{\text{estimated}} - \log_{10} K_{\text{measured}})}{N}$$
(43)

$$RE = \frac{\sum \left| \frac{\log_{10} K_{\text{estimated}} - \log_{10} K_{\text{measured}}}{\log_{10} K_{\text{measured}}} \right|}{N} \times 100\%$$
(44)

$$RMSE = \sqrt{\frac{\sum \left(\log_{10} K_{\text{estimated}} - \log_{10} K_{\text{measured}}\right)^{2}}{N}}$$
(45)

$$R^{2} = 1 - \frac{\sum \left(\log_{10} K_{\text{estimated}} - \log_{10} K_{\text{measured}}\right)^{2}}{\sum \left(\log_{10} K_{\text{estimated}} - \frac{1}{N} \sum \log_{10} K_{\text{estimated}}\right)^{2}}$$
(46)

where N is the number of data points, and $K_{\text{estimated}}$ and K_{measured} are the model estimates and measured values, respectively. As described earlier, logarithm values of K were used in Equations 43–46 to avoid deviations toward large K values in the wet range. Results of Equations 43–46 were presented as averages for each textural grouping and as averages for each data set.

Table 2Ranges of Basic Properties for the Soils Included in the Calibration and Validation Data Sets

Data set	Sand content (g g ⁻¹)	Clay content (g g ⁻¹)	Bulk density (g cm ⁻³)	Organic matter content (%)	$K_{\rm sat}$ (m s ⁻¹)
Max (calibration)	0.97	0.58	1.83	4	5.75×10^{-4}
Min (calibration)	0.03	0.01	0.49	0.04	5.56×10^{-8}
Max (validation)	1.00	0.63	1.75	5.9	3.09×10^{-4}
Min (validation)	0.00	0	0.46	0.04	4.63×10^{-8}

4. Results and Discussion

4.1. Optimization Results

Two models, the new hydraulic conductivity model (Equation 35) and the MVG model (Equation 39), were fitted to the $K(\theta, \psi)$ values of each soil sample in the calibration data set to determine the model parameters. Figure 4 displays the Equations 35 and 39 fitted K values versus the measured values. Overall, the Equation 35 values distributed more closely along the 1:1 line, the slope of the regression line was closer to unity, and the intercept was closer to zero than for the Equation 39 values. This performance is attributed to the flexible form of Equation 35, in contrast to the MVG model which is constrained by a given $\theta(\psi)$ function. Our new K model is a function independent of θ and ψ values which naturally improves its ability to fit measurements. For the calibration data set, the ME, RE, RMSE, and

FU ET AL. 11 of 25

19447973, 2023, 6, Downloaded from https://agupubs.onlinelibrary.wiley.com/doi/10.1029/2022WR034186 by North Carolina State Universit, Wiley Online Library

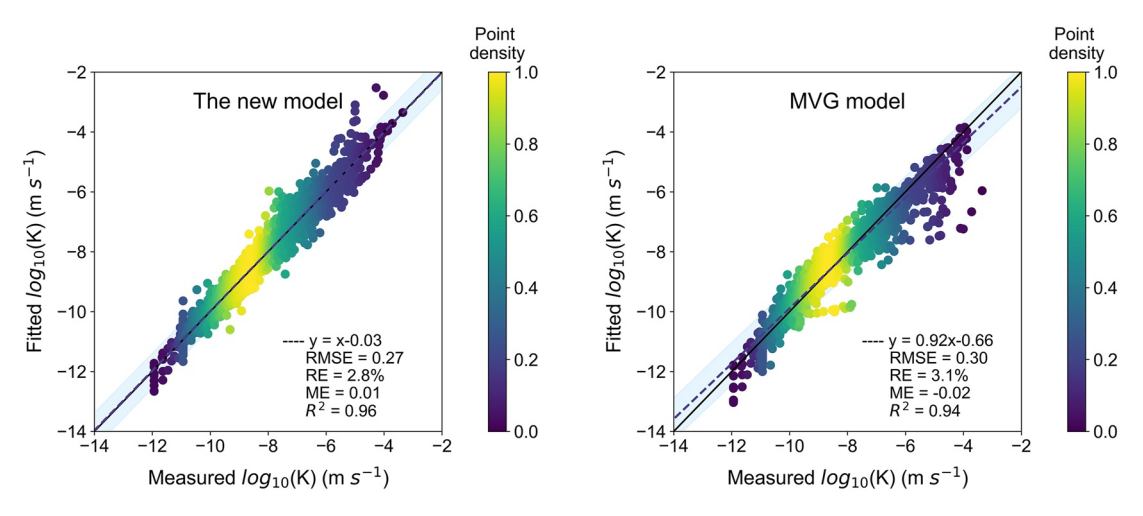


Figure 4. Soil hydraulic conductivity $(\log_{10}(K))$ values fitted by the new hydraulic conductivity model (Equation 35) with fitted c and γ and Mualem-van Genuchten model (Equation 39) with fitted K_0 and q versus the measured values of $\log_{10}(K)$ for 150 soils in the calibration data set. The solid lines are the 1:1 lines, the dashed lines represent the regression lines, and the blue regions indicate 95% prediction intervals.

the R^2 values between the fitted results with Equation 35 and the measured K values (in log scale) were 0.01, 2.8%, 0.27, and 0.96, respectively, and the corresponding values of Equation 39 were -0.02, 3.1%, 0.30, and 0.94, respectively. All metrics indicated that the new model performed better than the MVG model. The most obvious difference between two models appeared on high $\log_{10}(K)$ values: the new model overestimated on several soils without available K_{sat} information which was applied as the upper limit to avoid unrealistic high estimation near saturation; in contrast, MVG model significantly underestimated at wet region as it used K_0 as a matching point, which was generally one order of magnitude smaller than K_{sat} (Luckner et al., 1989), to yield better fitting results at more negative ψ values (i.e., lower $\log_{10}(K)$ values) but lost the accuracy near saturation, which was consistent with the findings of Schaap et al. (2001).

4.2. Correlation Between Fitting Parameters With Soil Properties

We obtained the values of parameter c and γ by fitting Equation 35 to the $K(\theta, \psi)$ datapoints of soils in the calibration data set. As the spread of c was several orders of magnitude, logarithmic values of c (log₁₀(c)) were used. For 150 soils in the calibration data set, our fitting results yields $\log_{10}(c)$ ranging from -14.88 to 1.22 with a SD of 3.35 and γ ranging from -21.16 to 8.20 with a SD of 5.88.

We further correlated parameters $\log_{10}(c)$ and γ with basic soil properties for all the soils in the calibration data set. In Figure 5, it appeared that no correlation existed between parameter $\log_{10}(c)$ and γ with bulk density and organic OM with (R^2 of 0.06 and 0.08, respectively). However, positive correlations between parameters $\log_{10}(c)$ and γ with sand content ($R^2 = 0.41$ and 0.37, respectively) and negative correlations with clay content ($R^2 = 0.33$ and 0.29, respectively) are shown. The correlation between parameter $\log_{10}(c)$ with soil texture can be attributed to the variation of $(\lambda + 2)/(\lambda + 4)$ which increases with increasing sand content (with a R^2 of 0.44) and decreasing clay content (with a R^2 of 0.36) as shown in Figure S1 in Supporting Information S1. Recall that γ is the sum of the tortuosity exponent β and the saturation exponent n at high salinity limit or $\beta + n - 1$ at low salinity limit. We have shown that if n is fixed as 2, the tortuosity exponent β is identical to the tortuosity-connectivity factor in the Mualem-Brooks-Corey or Burdine-Brooks-Corey models. Thus, it is unsurprising that parameter γ increases with increasing sand content but decreasing clay content as similar correlations between the tortuosity-connectivity factor with sand content and clay content have been reported extensively by previous studies (Rudiyanto et al., 2021; Schaap & Leij, 2000; Vereecken, 1995). In this study, we obtained a range of γ from -21.16 to 8.20. This result is consistent with Yates et al. (1992), which have also reported a wide variability of the tortuosity-connectivity factor, ranging from -3.31 to greater than 100. We also found that the γ distribution was concentrated when sand content >0.5 g g⁻¹ or clay content <0.2 g g⁻¹ but showed a larger variability with deceasing sand content or increasing clay content. Interestingly, Schuh and Cline (1990) also found similar results for the tortuosity-connectivity factor q of the MVG model which distributed in a narrow range for mean

FU ET AL. 12 of 25

1944-7973, 2023, 6, Downboaded from https://agupubs.onlinelibrary.wiley.com/doi/10.1029/2022WR034186 by North Carolina State Universit, Wiley Online Library on [05/06/2023]. See the Terms and Conditions (https://onlinelibrary.wiley.com/doi/10.1029/2022WR034186 by North Carolina State Universit, Wiley Online Library on [05/06/2023]. See the Terms and Conditions (https://onlinelibrary.wiley.com/doi/10.1029/2022WR034186 by North Carolina State Universit, Wiley Online Library on [05/06/2023]. See the Terms and Conditions (https://onlinelibrary.wiley.com/doi/10.1029/2022WR034186 by North Carolina State Universit, Wiley Online Library on [05/06/2023]. See the Terms and Conditions (https://onlinelibrary.wiley.com/doi/10.1029/2022WR034186 by North Carolina State Universit, Wiley Online Library on [05/06/2023]. See the Terms and Conditions (https://onlinelibrary.wiley.com/doi/10.1029/2022WR034186 by North Carolina State Universit, Wiley Online Library on [05/06/2023]. See the Terms and Conditions (https://onlinelibrary.wiley.com/doi/10.1029/2022WR034186 by North Carolina State Universit, Wiley Online Library on [05/06/2023]. See the Terms and Conditions (https://onlinelibrary.wiley.com/doi/10.1029/2022WR034186 by North Carolina State University (https://onlinelibrary.wiley.com/doi/10.1029/2

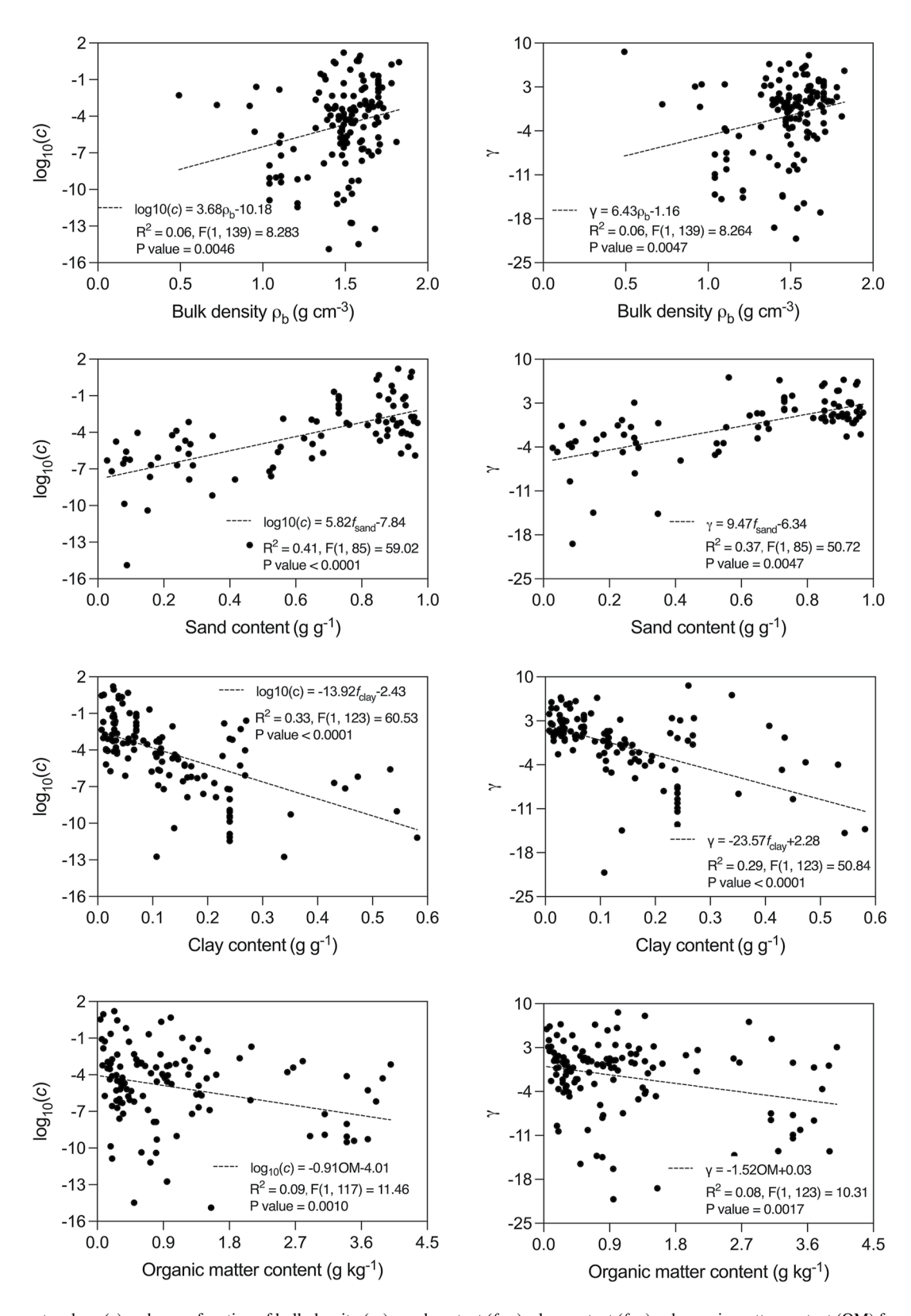


Figure 5. The parameters $\log_{10}(c)$ and γ as a function of bulk density (ρ_b) , sand content (f_{sand}) , clay content (f_{clay}) and organic matter content (OM) for soils in the calibration data set.

FU ET AL. 13 of 25

Table 3The Statistical Description of the Sand Content, Clay Content and Fitting $\log_{10}(c)$ and γ for Soils in Each Textural Group

	N		Max	Min	Mean	Median	SD
Group I	53	Sand content (g g ⁻¹)	0.97	0.82	0.91	0.91	0.04
		Clay content (g g ⁻¹)	0.07	0.01	0.03	0.03	0.02
		$\log_{10}(c)$ (unitless)	1.22	-6.11	-2.22	-2.35	1.90
		γ (unitless)	6.71	-2.31	2.20	1.66	2.15
Group II	26	Sand content (g g ⁻¹)	0.76	0.53	0.67	0.68	0.08
		Clay content (g g ⁻¹)	0.19	0.07	0.10	0.10	0.04
		$\log_{10}(c)$ (unitless)	-0.67	-10.35	-4.17	-3.68	2.36
		γ (unitless)	6.65	-10.14	0.18	0.63	3.48
Group III	61	Sand content (g g ⁻¹)	0.63	0.03	0.24	0.24	0.16
		Clay content (g g ⁻¹)	0.34	0.07	0.19	0.18	0.06
		$\log_{10}(c)$ (unitless)	-1.06	-14.88	-6.58	-6.20	3.26
		γ (unitless)	8.60	-21.16	-4.37	-3.07	6.56
Group IV	10	Sand content (g g ⁻¹)	0.24	0.09	0.16	0.16	0.11
		Clay content (g g ⁻¹)	0.58	0.34	0.45	0.44	0.08
		$\log_{10}(c)$ (unitless)	-3.34	-12.75	-7.47	-6.91	3.09
		γ (unitless)	2.19	-16.32	-7.34	-6.71	6.44

particle diameter $(D_{\rm m}) > 0.08$ mm but showed increasing variability for soils with $D_{\rm m} < 0.08$. Such a consistency again confirmed the intrinsic correlation between γ and q again. In summary, Figure 5 shows that the parameters $\log_{10}(c)$ and γ seem to correlate better with the different textural classes, suggesting that they are governed by the textural composition of the soils. However, for 199 soils in the calibration data set, only 104 of them have complete soil texture information (USDA system), and 93 of them have both complete texture and bulk density, 83 of them have complete texture, bulk density as well as organic OM, which are commonly used predictors for developing the PTF to estimate the hydraulic parameters (Looy et al., 2017; Vereecken et al., 2010). Thus, in this study, we split the data into subsets of different textural classes to minimize the prediction error.

4.3. Best-Fitted $\log_{10}(c)$ and γ Values

Previous analysis showed that both $\log_{10}(c)$ and γ had relatively strong correlation with sand content and clay content. Therefore, we divided all soils into four textural groupings based on their texture and values of fitting parameters: Group I (sand and loamy sand), Group II (sandy loam), Group III (sandy clay loam, loam, clay loam, silt loam, silt, and sandy clay), and Group IV (silty clay loam, silty clay, and clay). Interestingly, we found that the classification here is similar to the four Hydrological Soils Group (i.e., A, B, C, and D) based on runoff potential by the Natural Resource Conservation Service (NRCS, 1986). Besides, Schaap and Leij (2000) also divided all soils into four textural groups: sands, loams, silts, and clays. A detailed comparison between these classifications is provided in Table S1 in Supporting Information S1. The classification proposed in this study is somewhat a combination of texture-based and hydraulic-based methods (e.g., Ghanbarian & Yokeley, 2021; Twarakavi et al., 2010). The statistical descriptions of sand content, clay content and fitting $\log_{10}(c)$ and γ for the four textural groups are given in Table 3. Obviously, from Group I to Group IV, range and mean (or median) of sand content decreased but clay content increased. The fitted $\log_{10}(c)$ and γ values of the Group I had averages of -2.22 and 2.20, respectively, which was much higher than those of the other textural groupings (with averages of -4.17 and 0.18 for Group II, -6.58 and -4.37 for Group III, and -7.47 and -7.34 for Group IV). Again, if we assume a universal Archie's saturation exponent n of 2, the best-fitting γ values correspond to β of 0.20 for Group I, -1.82 for Group II, -6.37 for Group III and -9.34 for Group IV. We find that β results for Groups I (i.e., sand and loamy sand) and II (i.e., sandy loam) indirectly estimated from best-fitting γ values are not greatly different from the tortuosity-connectivity factor q of the MVG model for coarse-textured soils (-1)suggested by Schaap and Leij (2000). Additionally, the distribution of fitted $\log_{10}(c)$ and γ values of the Group I was relatively narrow (with SD of 1.90 and 2.15) but those of the other three groups were scattered (Figure S2 in

FU ET AL. 14 of 25

19447973, 2023, 6, Downloaded

doi/10.1029/2022WR034186 by North Carolina

Table 4

The Mean Error (ME), Relative Error (RE), Root Mean Square Error (RMSE) and Coefficient of Determination (R^2) Between $\log_{10}(K)$ (K in $m\ s^{-1}$) Estimated Values From the New Hydraulic Conductivity Model (Equation 35) With Best Fitting $\log_{10}(c)$ Values for Each Textural Group and Measured $\log_{10}(K)$ Values for Soils in Validation Data Sets 1 and 2

Validation data set	Group	N	ME (m s ⁻¹)	RE	RMSE (m s ⁻¹)	R^2
Data set 1	I	19	0.18	8.8%	0.76	0.76
	II	7	-0.14	6.5%	0.56	0.80
	III	21	0.10	8.4%	0.81	0.74
	IV	2	-1.19	14.1%	1.42	0.92
	Average	49	0.02	8.8%	0.80	0.73
Data set 2	I	9	-0.02	9.6%	0.77	0.88
	II	4	-0.15	7.7%	0.66	0.82
	III	7	-0.21	9.5%	0.77	0.80
	IV	3	0.19	4.0%	0.37	0.94
	Average	23	-0.01	9.5%	0.77	0.85
Average			0.01	9.1%	0.79	0.76

Note. N is the number of soil samples in each textural group.

Supporting Information S1). We also conducted an ANOVA analysis, and we found there were significant differences among the four textural group for the fitting parameters. Corresponding results are provided in Tables S3 and S4 in Supporting Information S1. We then determined the best fitting parameters to represent each textural group by fitting Equation 35 to the $K(\theta, \psi)$ data of soil samples of each textural group as a whole. The best fitting $\log_{10}(c)$ and γ results were -2.53 and 1.92, -4.39 and -0.14, -5.01 and -1.34, and -5.79 and -2.27 for Groups I–IV, respectively. These $\log_{10}(c)$ and γ values were then used to estimate K from the $\theta(\psi)$ data using Equation 35 for soils with known textural information.

4.4. Performance of the New Hydraulic Conductivity Model

We tested the new $K(\theta, \psi)$ relationship with validation data sets 1 and 2, in which the best fitting $\log_{10}(c)$ and γ values were used according to soil textural groupings. Table 4 presents the statistical parameters that indicate the performance of the $K(\theta, \psi)$ function. The new model provided reasonable K estimates for the soils in validation data set 1 with ME, RE, RMSE, and R^2 of 0.02, 8.8%, 0.80, and 0.73, respectively. In general, the new model provided satisfactory results in Group I, II, and III with ME ranging from -0.14 to 0.18, RE ranging from 6.5% to 8.8%, RMSE ranging from 0.56 to 0.81 and R^2 ranging from 0.74 to 0.80. Among the three groups, the new model performed best on Group II with lowest RE, lowest RMSE and highest R^2 . This maybe because Group II included sandy loam only which made the

best-fitting parameters for Group II more representative than other Groups. However, it was impossible to determine the best-fitting parameters for each textural class as some of them (e.g., clay) had only limited soils available in the UNSODA database. The new model also performed poorly on Group IV with ME, RE, and RMSE of -1.19, 14.1%, and 1.42, respectively.

The new $K(\theta, \psi)$ model also gave accurate K estimates on data set 2 with an ME of -0.02, a RE of 9.6%, a RMSE of 0.77 and an R^2 of 0.85 (Table 4). The performance of the new model on data set 2 showed consistent trends with data set 1: among Groups I–III the highest R^2 appeared on Group I and Group II had the lowest RMSE. However, the new model showed better performance on Group IV in data set 2. In this case, performance was best among the four groups with a lowest RE of 4.0%, a lowest RMSE of 0.37 and a highest R^2 of 0.94. Such different performance was mainly because of the large variability of fitting $\log_{10}(c)$ and γ values on fine-textured soils, thus it is unfair to use single best-fitting values to represent the whole Group IV. Additionally, there were only 10 soils for Group IV in the calibration, which may also limit the performance of the new model. Overall, the two metrics, ME and RE, indicated poorer performance for validation data set 2 than for data set 1, while the two metrics, RMSE and R^2 , showed better performance for validation data set 2 than for data set 1.

Figure 6 compares the new model estimated log10(K) values with the measured log10(K) values for data sets 1 and 2. In general, the data points of validation data set 1 distributed evenly but had scatter along the 1:1 line, whereas those of validation data set 2 were more concentrated but the regression line deviated from the 1:1 line, indicating that the new model provided reliable K data for the two validation data sets. The close performance among two data sets confirmed the good performance of the new model.

4.5. Model Uncertainty

To assess the new $K(\theta, \psi)$ model's uncertainty, the statistical results of best-fitting parameters for four textural groups, including best-fitting values, SD, lower and higher 95% confidence interval, are provided in Table S2 in Supporting Information S1. Figure 7 shows the uncertainty of estimation for four representative soils from the validation data set: UNSODA 4660 sand, Gilat sandy loam, UNSODA 4030 silt loam and Avignon silty clay loam, which correspond to Group I–IV, respectively. The results demonstrate that the estimates generally follow the pattern of the observed data. For three soils other than UNSODA 4660 sand, the largest uncertainty appears in the dry region and uncertainty at intermediate θ is smallest. The limited performance of the new model can be

FU ET AL. 15 of 25

19447973, 2023, 6, Downloaded from https://agupubs.onlinelib

com/doi/10.1029/2022WR034186 by North Carolina State Universit, Wiley Online Library on [05/06/2023]. See the Terms

and-conditions) on Wiley Online Library for rules of use; OA articles are governed by the applicable Creativ

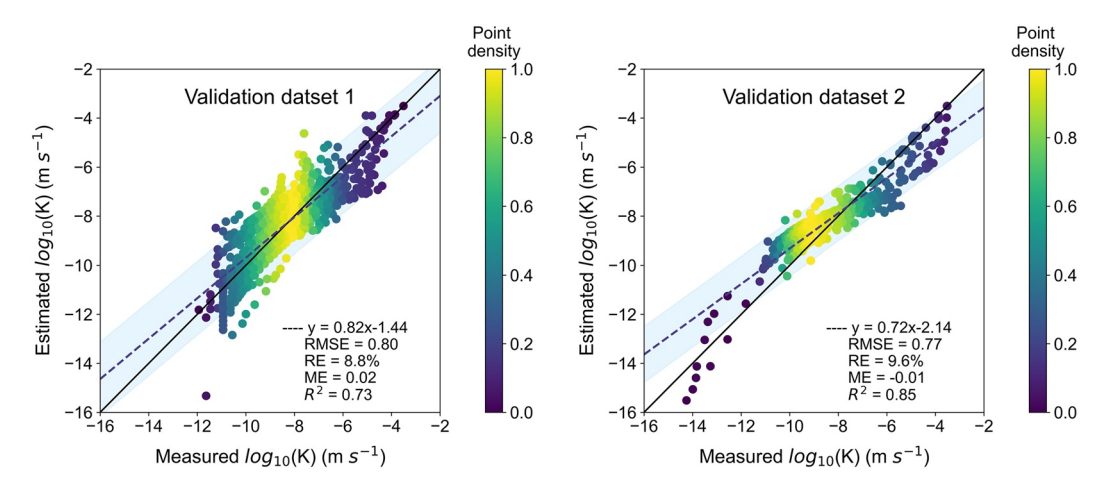


Figure 6. Comparison of $\log_{10}(K)$ estimated values with the new hydraulic conductivity model (Equation 35) with best fitting $\log_{10}(c)$ and γ values versus the measured $\log_{10}(K)$ values for soils in validation data set 1 and validation data set 2. The solid black lines are the 1:1 lines, the dashed lines are the regression lines, and the blue regions indicate 95% prediction intervals.

attributed to the following limitations: (a) the model produces unrealistically high K estimates near saturation; (b) film and vapor conductivity are not accounted for in the dry range; (c) soils are only classified into four textural groups, which is a coarse classification. In the following section, we will discuss these limitations in detail and explore ways to overcome them.

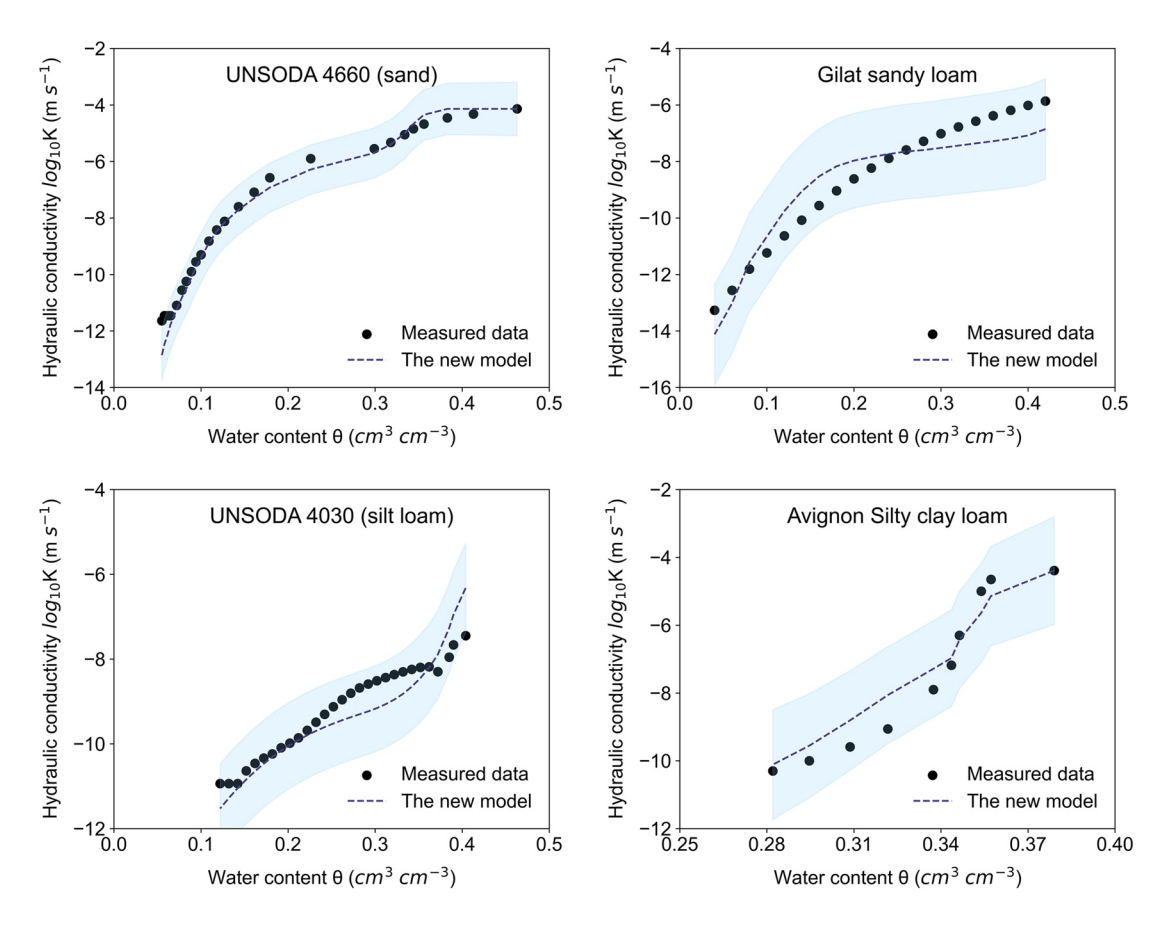


Figure 7. The uncertainty of the new model (Equation 35) for $K(\theta)$ curves of four representative soils in the validation data set. Black points represent the measured data, blue dash lines represent the new model estimate with best-fitting parameters and blue regions represent the 95% prediction intervals.

FU ET AL. 16 of 25

19447973, 2023, 6, Downloaded

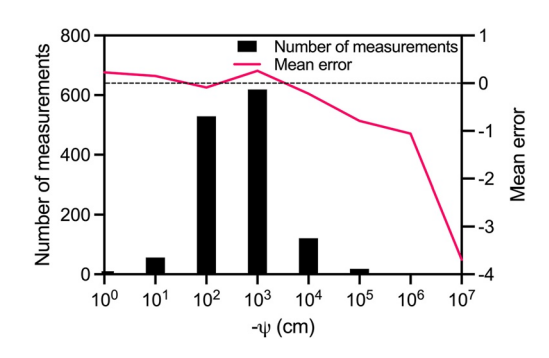


Figure 8. Mean error (ME) of the new model (Equation 35) for eight matric potential (ψ) classes. Note that ME results are calculated from soils in the validation results whereas number of soils observed in each matric potential classes are from the calibration data set.

4.6. Limitations of the New Model

Figure 8 shows the MEs obtained with the new model (Equation 35) for nine matric potential classes. A negative ME value indicates an underestimation of K ($\log_{10}K$), whereas a positive value denotes an overestimation. It is obvious that the new model overestimated K in the matric potential range from 0 to -10 cm. Recall that, when ψ approaches 0, estimated K with Equation 34 increases dramatically. We used $K_{\rm sat}$ as the upper constraint of Equation 34 because it was available for most soils in our study. However, a lower upper limit at lower ψ instead of $K_{\rm sat}$ would be better, especially for structured media (e.g., macroporous soils or fractured rock) where the macropore flow was significant but could not be well accounted for by Equation 35. The new model estimated the K accurately from -10 to -1,000 cm where MEs were nearly zero. This range was where most measurements in the calibration data set were distributed. The calibration inevitably enhanced the performance of the new model in this range. When ψ was below -1,000 cm, the new model consistently underestimated K values. This underestimation became more

severe as ψ decreased and ME could be as low as -3.7 when $\psi < -10^6$ cm. In this range, the underestimation of the new model was likely caused by two factors. First, as we stated above, the major distribution of the datapoints in the matric potential range between -10 and -1,000 cm reduced the new model applicability in other ψ ranges. Second, the new model was developed based on the Brooks-Corey model and the capillary bundle model which only accounted for capillary flow but ignored water adsorption, and film and corner flow (Tuller & Or, 2001). These omissions contributed to new model underestimations at low ψ values where soil water transport was mainly controlled by film flow.

In summary, the results presented in Figure 8 clearly highlight the limitations of the new model at both wet and dry ends. To overcome the former issue, a small minimum capillary matric potential (ψ_s , e.g., -1 cm) and a fictitious (extrapolated) parameter θ_m have been introduced, as reported by Ippisch et al. (2006) and Vogel et al. (2000), or a maximum pore size in the capillary bundle model, as suggested by Iden et al. (2015). While beyond the scope of this study, it is worth noting that better estimates near saturation could be obtained if a maximum hydraulic conductivity at a fixed matric potential near saturation was used as the upper limit in Equation 35, instead of K_{sat} . Moreover, various models have been proposed to account for the existence of film and vapor conductivity (Lebeau & Konrad, 2010; Peters, 2013; Peters et al., 2021; Tokunaga, 2009; Wang et al., 2022; Z. F. Zhang, 2011). The proposed model in this study was established using the capillary tube model, which can naturally capture the capillary flow only. The addition of film and vapor conductivity terms, as proposed by these studies, if coupled with the proposed model, may lead to improved model performance in the dry range. Unfortunately, the calibration data set was limited to the UNSODA data set in which $K(\theta, \psi)$ data points were mainly

Table 5The Mean Error (ME), Relative Error (RE), Root Mean Square Error (RMSE) and Coefficient of Determination (R^2) Between $\log_{10}(K)$ (K in m s $^{-1}$) Estimated Values From the New Hydraulic Conductivity Model (Equation 35) Using Best Fitting $\log_{10}(c)$ and γ Values or by the Mualem-Van Genuchten Model (Equation 39) for Five Cases for Each Textural Group Versus the Measured $\log_{10}(K)$ Values for Soils in the (Reduced) Validation Data Sets

	ME	RE	RMSE	R^2
-	0.01	9.1%	0.79	0.76
Case 1ª	-0.19	14.2%	1.55	0.47
Case 2ª	0.21	12.9%	1.29	0.51
Case 3 ^a	0.20	13.0%	1.26	0.58
Case 4	-0.16	12.0%	1.00	0.59
Case 5	-0.15	11.8%	1.00	0.59
	Case 2 ^a Case 3 ^a Case 4	- 0.01 Case 1 ^a -0.19 Case 2 ^a 0.21 Case 3 ^a 0.20 Case 4 -0.16	- 0.01 9.1% Case 1 ^a -0.19 14.2% Case 2 ^a 0.21 12.9% Case 3 ^a 0.20 13.0% Case 4 -0.16 12.0%	- 0.01 9.1% 0.79 Case 1 ^a -0.19 14.2% 1.55 Case 2 ^a 0.21 12.9% 1.29 Case 3 ^a 0.20 13.0% 1.26 Case 4 -0.16 12.0% 1.00

^aReduced data set including only 85 soils with known K_{sat} values.

distributed around the matric potential range -10 to -1,000 cm, as shown in Figure 8. Thus, the inclusion of other soil hydraulic properties data set (e.g., Weynants et al., 2013) is required for future calibration.

4.7. Comparison With Mualem-Van Genuchten Model

We further compared the performance of the new $K(\theta, \psi)$ model to the results from the MVG model with the validation data sets (Table 5). We tested the performance of the MVG model in five cases: (1) $K_0 = K_{\rm sat}$, q = 0.5; (2) $K_0 = K_{\rm sat}$, single q fitted from the whole calibration data set; (3) $K_0 = K_{\rm sat}$, variable q values for four textural groups fitted from the calibration data set; (4) single K_0 and q fitted from the whole calibration data set; and (5) variable K_0 and q values for four textural groups fitted from the calibration data set. A comparison of all models for validation data set 2 is also shown in Figure 9. For cases (1)–(3), only soils with known $K_{\rm sat}$ values were used, which resulted in a reduced calibration data set of 84 soils and a reduced validation of 48 soils. For the validation data set, it was apparent that the new model was superior to the MVG model: The ME, RE, RMSE, and R^2 of

FU ET AL. 17 of 25

1944/793, 2023, 6, Downloaded from https://agupubs.onlinelibrary.wiley.com/doi/10.109/2022WR034186 by North Carlina State Universit, Wiley Online Library on [05/06/2023]. See the Terms and Conditions (https://onlinelibrary.wiley.com/terms-and-conditions) on Wiley Online Library for utees of use; OA articles are governed by the applicable Cerative Common [05/06/2023]. See the Terms and Conditions (https://onlinelibrary.wiley.com/terms-and-conditions) on Wiley Online Library for utees of use; OA articles are governed by the applicable Cerative Common [05/06/2023].

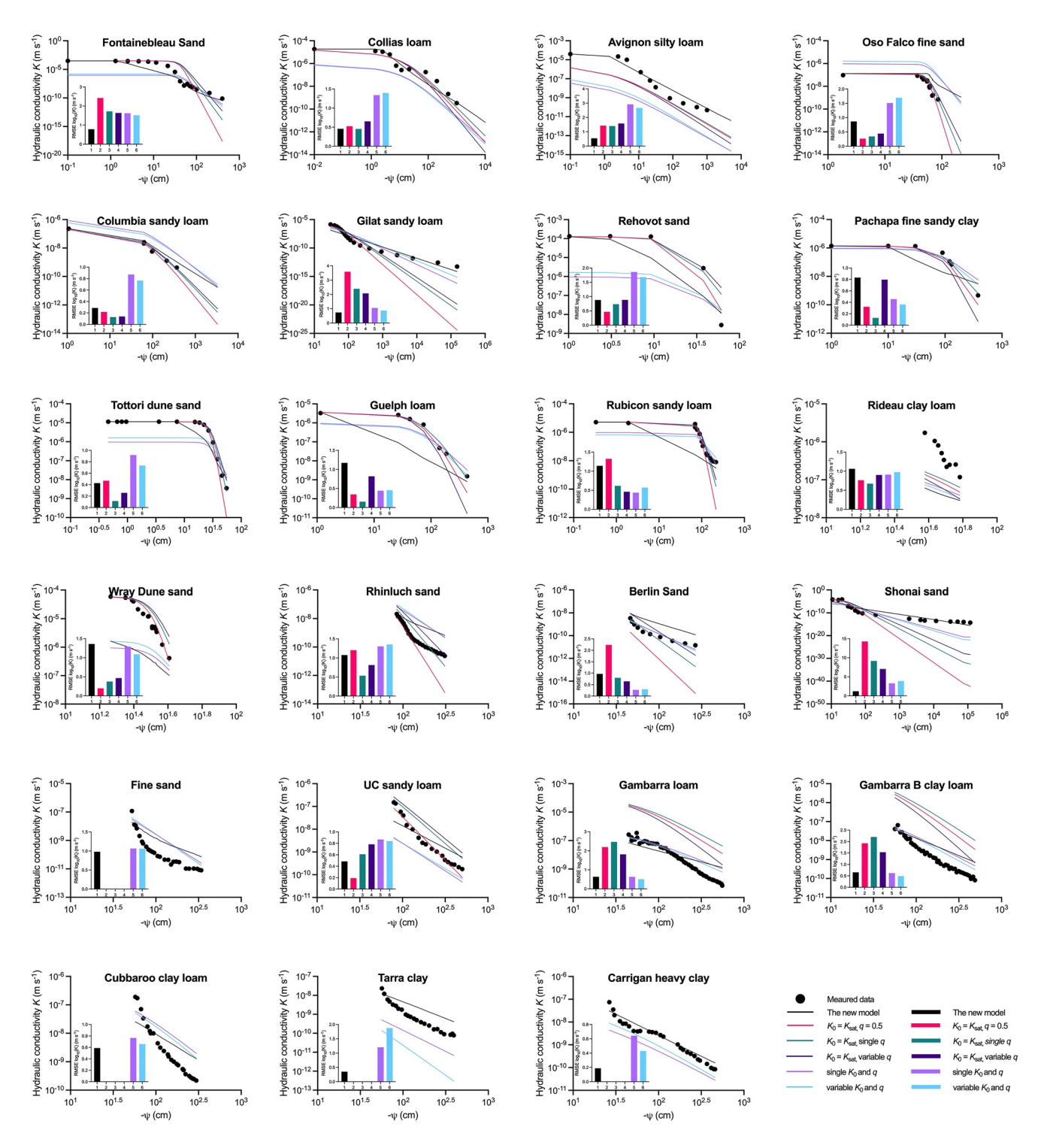


Figure 9. Comparison of the new model (Equation 35) and the Mualem-van Genuchten (MVG) model (Equation 39) for five cases on 23 soils in the validation data set 2. Bars in the bar charts indicate values for RMSE($\log_{10}(K)$) for the six applied model settings. (1) The new model; (2) MVG ($K_0 = K_{\text{sat}}$, q = 0.5); (3) MVG ($K_0 = K_{\text{sat}}$, variable q); (5) MVG (single K_0 and q); (6) MVG (variable K_0 and K_0).

the new model estimated $\log_{10}(K)$ values were -0.01, 8.8%, 0.78, and 0.76, respectively, and the corresponding values of the MVG model (when $K_0 = K_{\text{sat}}$, q = 0.5) were -0.19, 14.2%, 1.55, and 0.47, respectively. Then we fitted q values for the calibration data set, which were -0.28 in Case 2. In Case 3, the q values were -0.61, -0.51, 1.66, and 4.22 for Group I, Group II, Group III, and Group IV, respectively. When these calibrated q values were

FU ET AL. 18 of 25

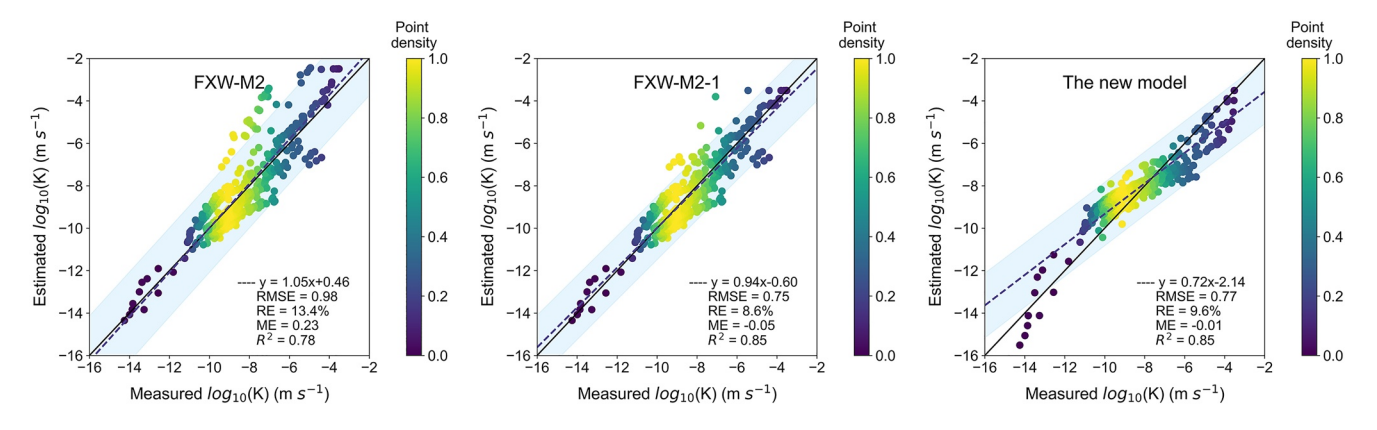


Figure 10. Comparison of $\log_{10}(K)$ estimated values with the FXW-M2 model (Wang et al., 2022), FXW-M2-1 model (FXW-M2 model with measured K_{sat} as upper limit) and new hydraulic conductivity model (Equation 35) with best fitting $\log_{10}(c)$ and γ values versus the measured $\log_{10}(K)$ values for soils in validation data set 2. The solid black lines are the 1:1 lines, the dashed lines are the regression lines, and the blue regions indicate 95% prediction intervals.

used, the results became better with ME of 0.20, RE of 13.0%, RMSE of 1.26 and R^2 of 0.58. We further fitted both $\log_{10}(K_0)$ and q and determined the single best-fitting values for the calibration data set, which were -6.02 and -1.38, respectively (Case 4). For Case 5, as what we did for the new model, we divided all soils into four textural groups and obtained best-fitting $\log_{10}(K_0)$ and q values of -5.79 and -1.26 for Group I, -6.18 and -1.66 for Group II, -6.05 and -1.11 for Group III, and -5.66 and 1.02 for Group IV. When both K_0 and q were fitted (i.e., cases 4 and 5), the performance of the MVG model was significantly improved (i.e., ME = -0.16 to -0.15, RE = 11.8%–12.0%, RMSE = 1.00 and $R^2 = 0.58$), which, however, was still much worse than the performance of the new model.

Additionally, to estimate K with the MVG model, requires fitting parameters S_e and n of the van Genuchten model, which, in turn, requires several pairs of $\theta(\psi)$ data points from a wide matric potential range to match the observed data. Obtaining such data is generally time consuming, which limits the successful application of the MVG model. In contrast, as soon as the best fitting $\log_{10}(c)$ and γ values are available, the new model is able to estimate K with a single $\theta(\psi)$ data point.

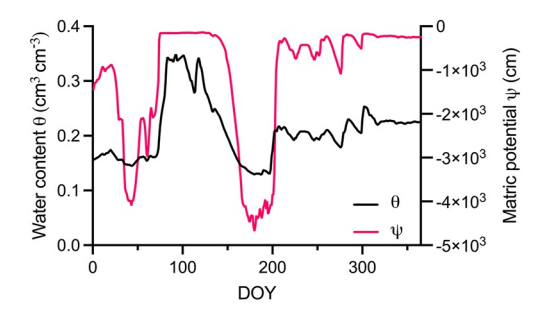
We also sought to compare the new $K(\theta, \psi)$ model with two widely used PTFs. Although there are numerous PTFs to estimate MVG model parameters, only a few of them have been validated using independent data sets (Vereecken et al., 2010). Most PTFs require basic soil properties such as texture, bulk density, organic OM and/or θ values at specific matric potentials; and not all of these parameters are available for most soils in our validation data set. Thus, it was not possible to directly compare these PTF results with the new model results using the same validation data set. Therefore, we compared the new model to two published PTFs, ROSETTA 3 (X. Zhang & Schaap, 2017) and Brunswick-Weber (BW) (Weber et al., 2020) using a reduced validation data set 2 consisting of 16 soils. With soil texture and bulk density as inputs, the two PTFs produced RMSEs (1.35 and 1.42), MEs (0.06 and 1.11) and REs (12.5% and 15.7%), respectively (results are presented in Figure S3 in Supporting Information S1). In comparison, the new model performs much better with RMSE of 0.70, ME of 0.14 and RE of 8.1% for the same validation data set.

Furthermore, we conducted a comparative analysis of our proposed model with the FXW-M2 model developed by Wang et al. (2022), using the independent validation data set 2. The results presented in Figure 10, demonstrate that our model outperformed the FXW-M2 model on several metrics. Specifically, our model yielded a lower root mean squared error (RMSE) of 0.77 compared to 0.98 for the FXW-M2 model, a lower RE of 9.6% compared to 13.4%, and a model error (ME) closer to 0 (-0.01 vs. 0.23) as well as a higher R^2 value of 0.85 compared to 0.78 for the FXW-M2 model. It is noteworthy that the regression line for the FXW-M2 model had a slope closer to unity and an intercept closer to zero, indicating its better performance at extremely low (dry range) and high (near saturation) K range. This outperformance can be attributed to the fact that the FXW-M2 model accounts for both capillary and film water, and also incorporates a fixed matric potential (i.e., -1 cm) to enhance its performance near saturation. The unexpected overestimation of datapoints near saturation in the FXW-M2 model is due to errors in the indirect estimation of $K_{\rm sat}$ using Equation 14 in their study. This approach reduced the required input (i.e., $K_{\rm sat}$) but yielded unrealistic high K values, leading to the overestimation. To ensure a fair comparison, we used measured $K_{\rm sat}$ as the upper limit when applying the FXW-M2 model and referred to the resulting model as

FU ET AL. 19 of 25

19447973, 2023, 6, Downloaded from https

com/doi/10.1029/2022WR034186 by North Carolina State Universit,



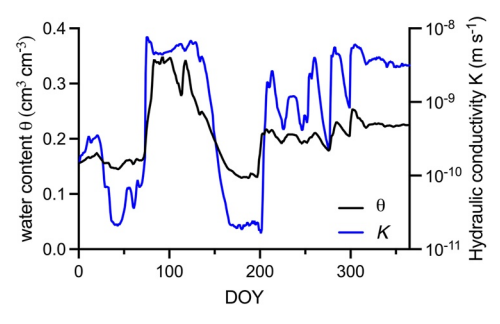


Figure 11. Daily average of water content (θ) , matric potential (ψ) and hydraulic conductivity (K) on a loamy soil at 12-cm depth in the Mixed Conifer Zero Order Basin site in 2011. DOY refers to day of year. K data are estimated from θ and ψ using the new model (Equation 35).

FXW-M2-1. The results presented in Figure 10 clearly support our analysis, as the performance of the FXW-M2-1 model improved significantly, particularly in the high K range, with an RMSE of 0.75, RE of 8.6%, ME of -0.05, and R^2 of 0.85. It is surprising that the new model's performance is comparable to that of the FXW-M2-1 model, despite not considering film flow near the dry end or introducing fixed matric potential, as Wang et al. (2022) and other related studies have done. This close performance attested to the accuracy of the new model and underscored its considerable potential, particularly once the limitations discussed in Section 4.6 are addressed in future studies.

5. Further Discussion

5.1. Implications of the Proposed $K(\theta, \psi)$ Relationship

In this study, we propose a $K(\theta, \psi)$ relationship that integrates the capillary bundle model, the Brooks-Corey model, and the Waxman and Smits model. The implications of this $K(\theta, \psi)$ relationship are significant and range from laboratory to field-scale applications. In the laboratory, determining soil hydraulic properties using steady-state or transient-state methods can be tedious, expensive, and time-consuming (Hill, 2004). Prior studies have utilized inverse modeling of multistep outflow or Schindler's method to simultaneously measure the SWRC and HCC, which is often limited to a relatively narrow range of water content and matric potential due to the restrictions of tensiometers (e.g., Bahrami et al., 2020; Durner & Iden, 2011; Schindler et al., 2010; van Dam et al., 1994; Wildenschild et al., 2001). Consequently, it can be challenging to determine the corresponding K at low matric potential (<-1,000 cm) where SWRCs can be determined using a pressure-chamber

or dew point potentiometer. As shown in Figure 7, most measurements in the calibration data set are concentrated between -100 and -1,000 cm, reinforcing this limitation. Furthermore, this also restricts the application of functions between SWRC and HCC (e.g., MVG model) as they require fitting the SWRC parameters first using a wide range of (θ, ψ) data. In contrast, the newly proposed $K(\theta, \psi)$ relationship has the capability to determine K using just a single pair of θ - ψ data, which is especially crucial when there are limited SWRC data available.

The significance of the proposed $K(\theta, \psi)$ relationship becomes more evident under field conditions. Infiltration experiments using devices such as tension disc infiltrometer and pressure ring infiltrometers have been developed to determine K in the field (Ankeny et al., 1991). However, these methods cannot provide continuous in-situ K dynamics. Fortunately, emerging sensing technologies such as time-domain reflectometry and matric potential sensors (tensiometers and psychrometers) can provide continuous in-situ θ and ψ measurements (Fu et al., 2020; Reece, 1996; Robinson et al., 2008; M. Zhang et al., 2017). By coupling these modern technologies with the proposed $K(\theta, \psi)$ relationship, it is now possible to determine the in-situ K dynamics. An example application is shown in Figure 11: continuous θ and ψ measurements were obtained using Decagon 5TE and MPS-1 sensors (Pullman, WA) on a loamy soil at 12 cm depth located in the Mixed Conifer Zero Order Basin (ZOB), Jemez River Basin, New Mexico. Further details about measurements and site information can be referred to Schaap et al. (2021). Using the proposed model (Equation 35) with best-fitting $\log_{10}(c)$ and γ of -6.58 and -4.37, respectively, for loamy soil (Group III), we estimated the K dynamics from θ and ψ data. However, we were unable to evaluate the reliability of our model estimates as no independent K measurements were available in this study. Future studies should investigate this further.

5.2. Implications of the Proposed $K(\sigma, \theta, \psi)$ Relationship

In the initial stages of the model development section, we began with the capillary tube bundle model and established a K- σ relationship for two salinity extremes. We realized that there were limited joint measurements of soil hydraulic and electrical properties for most soils, thus we further developed a $K(\theta, \psi)$ relationship (Equation 35) further. However, the proposed $K(\sigma, \theta, \psi)$ relationship does have its merit in practical applications and needs to be discussed here. It can be expressed as follows:

$$K = 2.71 \times 10^{-4} \frac{c}{\psi^2} \theta^{\beta} \frac{\sigma_{\rm u}}{\sigma_{\rm w}}$$
 High salinity: $\frac{\sigma_{\rm w}}{\sigma_{\rm EDL}} \to \infty$ (47a)

FU ET AL. 20 of 25

As discussed previously, Equation 47a can be compared to the K- σ relationships proposed in several previous studies, including Doussan and Ruy (2009), Ghanbarian et al. (2017), Niu et al. (2015), and Revil et al. (2014). While the fundamental expression of the relationships is similar, there are differences in their coefficients and length scales. The correlation between different length scales has been proposed in Equation 18, and the variation in coefficients can be attributed to differing assumptions regarding the shape of the pores (e.g., pore length being equal to pore diameter or independent; cylindrical or slit-shaped pores). While a comprehensive discussion of these differences is beyond the scope of this study, interested readers can refer to Skaggs (2011) and Ghanbarian et al. (2016) for more information. Two highlights regarding the proposed $K(\sigma, \theta, \psi)$ need be addressed here. First, previous studies assumed the same tortuosity or critical radius for electrical current and water flow, which is only valid for a homogenous porous medium or one with infinite pore size distribution. However, we have taken this difference into account by introducing a tortuosity correction factor (θ^{β}) into the K- σ then justifying its connection to the tortuosity factor in the Mualem (1976) model. Second, previous studies usually ignored the effects of surface conduction or treated it as a perturbation to pore water conduction while developing the K- σ relationships. In this study, we proposed a K- σ relationship for two salinity extremes. Future work will aim to fill the transitional region (e.g., by employing a Padé approximant) and forge a more general relationship valid over the whole salinity range, then Equation 47 can be effectively applied to agricultural soils where soil salinity levels are typically low to medium. At the field scale, several geophysical methods, such as direct current resistivity and electromagnetic induction can be used to determine the electrical conductivity at a different depth (Binley et al., 2015). Coupling any of them with matric potential sensors, the proposed $K(\sigma, \theta, \psi)$ relationship could possibly enable the in-situ K estimates at dynamic spatial and temporal scales.

6. Conclusion

We derived a new $K(\theta, \psi)$ relationship based on the capillary bundle model, the Brooks-Corey model, and Waxman and Smits model. We used measured $K(\theta, \psi)$ values from 150 soils to obtain the best fitted model parameters for four textural groupings. The new model, which used these two fitting parameters and a θ and ψ pair as the inputs, provided accurate estimates of K for 72 soils from two validation data sets. Compared to the MVG model, which was constrained by a required $\theta(\psi)$ function, the new $K(\theta, \psi)$ model could estimate K values from individual θ and ψ data pairs, and the new model provided more accurate results. Additional comparisons to ROSETTA 3 and BW PTFs also indicated the reliability of the new model. While further investigation is needed through both theoretical analysis to overcome its limitations and experimentally testing, particularly at the field scale, the proposed model offers potential for estimating K in a range of hydrologic studies.

Data Availability Statement

The hydraulic conductivity and water retention curve data for the 171 soils used in the calibration data set and validation data set 1 are from the UNSODA database (Nemes et al., 2001). The data for the 23 soils used in the validation data set 2 were collected as follows: Fontainebleau sand, Collias loam and Avignon silty clay loam (Doussan & Ruy, 2009); Oso Falco fine sand and Columbia sandy loam (Tuli & Hopmans, 2004); Gilat sandy loam, Rehovot sand and Pachapa Fine sandy clay (Mualem, 1976); Tottori dune sand (Sakai & Toride, 2007); Guelp loam (Elrick & Bowman, 1964); Rubicon sandy loam (Topp, 1969); Rideau clay loam (Topp, 1971); Wray Dune sand (Gillham et al., 1979); Rhinluch sand (Schindler & Müller, 2006); Berlin sand (Peters, 2013); Shonai sand (Mehta et al., 1994); Fine sand, UC sandy loam, Gambarra loam, Gambarra B clay loam, Cubbaroo clay loam, Tarra clay, and Carrigan heavy clay (Minasny & Field, 2005). All of the data used in this study can be found in Fu et al. (2023).

References

Ankeny, M. D., Ahmed, M., Kaspar, T. C., & Horton, R. (1991). Simple field method for determining unsaturated hydraulic conductivity. Soil Science Society of America Journal, 55(2), 467–470. https://doi.org/10.2136/sssaj1991.03615995005500020028x
Assouline, S. (2001). A model for soil relative hydraulic conductivity based on the water retention characteristic curve. Water Resources Research, 37(2), 265–271. https://doi.org/10.1029/2000wr900254

Acknowledgments
This research was so

This research was supported by the US National Science Foundation (Grant: 2037504) and USDA-NIFA Multi-State Project 4188. The authors would like to thank eight anonymous reviewers and, in particular, to the Associate Editor, Andrew Binley, for their constructive criticisms and helpful comments, which led to major improvements of this paper.

FU ET AL.

21 of 25



- Assouline, S. (2006). Modeling the relationship between soil bulk density and the hydraulic conductivity function. *Vadose Zone Journal*, 5(2), 697–705. https://doi.org/10.2136/vzj2005.0084
- Bahrami, A., Aghamir, F., Bahrami, M., & Khodaverdiloo, H. (2020). Inverse modeling towards parameter estimation of the nonlinear soil hydraulic functions using developed multistep outflow procedure. *Journal of Hydrology*, 590, 125446. https://doi.org/10.1016/j.jhydrol.2020.125446
- Banavar, J. R., & Johnson, D. L. (1987). Characteristic pore sizes and transport in porous media. Physical Review B, 35(13), 7283–7286. https://doi.org/10.1103/physrevb.35.7283
- Binley, A., Hubbard, S. S., Huisman, J. A., Revil, A., Robinson, D. A., Singha, K., & Slater, L. D. (2015). The emergence of hydrogeophysics for improved understanding of subsurface processes over multiple scales. *Water Resources Research*, 51(6), 3837–3866. https://doi.org/10.1002/2015wr017016
- Binley, A., & Slater, L. (2020). Resistivity and induced polarization: Theory and applications to the near-surface Earth. Cambridge University

 Press
- Børgesen, C. D., Iversen, B. V., Jacobsen, O. H., & Schaap, M. G. (2008). Pedotransfer functions estimating soil hydraulic properties using different soil parameters. Hydrological Processes, 22(11), 1630–1639. https://doi.org/10.1002/hyp.6731
- Brooks, R. H., & Corey, A. T. (1964). Hydraulic properties of porous media and their relation to drainage design. *Transactions of the ASAE*, 7(1), 0026–0028. https://doi.org/10.13031/2013.40684
- Burdine, N. T. (1953). Relative permeability calculations from pore size distribution data. *Journal of Petroleum Technology*, 5(03), 71–78. https://doi.org/10.2118/225-g
- Campbell, G. S. (1974). A simple method for determining unsaturated conductivity from moisture retention data. Soil Science, 117(6), 311–314. https://doi.org/10.1097/00010694-197406000-00001
- Coleman, S. W., & Vassilicos, J. C. (2008). Transport properties of saturated and unsaturated porous fractal materials. *Physical Review Letters*, 100(3), 035504. https://doi.org/10.1103/physrevlett.100.035504
- Cui, Y. J., Tang, A. M., Loiseau, C., & Delage, P. (2008). Determining the unsaturated hydraulic conductivity of a compacted sand–bentonite mixture under constant-volume and free-swell conditions. *Physics and Chemistry of the Earth, Parts A/B/C*, 33, S462–S471. https://doi. org/10.1016/j.pce.2008.10.017
- David, C. (1993). Geometry of flow paths for fluid transport in rocks. *Journal of Geophysical Research*, 98(B7), 12267–12278. https://doi.org/10.1029/93jb00522
- David, C., Gueguen, Y., & Pampoukis, G. (1990). Effective medium theory and network theory applied to the transport properties of rock. *Journal of Geophysical Research*, 95(B5), 6993–7005. https://doi.org/10.1029/jb095ib05p06993
- Doussan, C., & Ruy, S. (2009). Prediction of unsaturated soil hydraulic conductivity with electrical conductivity. *Water Resources Research*, 45(10), W10408. https://doi.org/10.1029/2008wr007309
- Doyen, P. M. (1988). Permeability, conductivity, and pore geometry of sandstone. *Journal of Geophysical Research*, 93(B7), 7729–7740. https://doi.org/10.1029/jb093jb07p07729
- Durner, W., & Iden, S. C. (2011). Extended multistep outflow method for the accurate determination of soil hydraulic properties near water saturation. Water Resources Research, 47(8), W08526. https://doi.org/10.1029/2011wr010632
- Eching, S. O., Hopmans, J. W., & Wendroth, O. (1994). Unsaturated hydraulic conductivity from transient multistep outflow and soil water pressure data. *Soil Science Society of America Journal*, 58(3), 687–695. https://doi.org/10.2136/sssaj1994.03615995005800030008x
- Elrick, D. E., & Bowman, D. H. (1964). Note on an improved apparatus for soil moisture flow measurements. Soil Science Society of America Journal, 28(3), 450–453. https://doi.org/10.2136/sssaj1964.03615995002800030045x
- Ewing, R. P., & Hunt, A. G. (2006). Dependence of the electrical conductivity on saturation in real porous media. *Vadose Zone Journal*, 5(2), 731–741. https://doi.org/10.2136/vzj2005.0107
- Friedman, S. P. (2005). Soil properties influencing apparent electrical conductivity: A review. *Computers and Electronics in Agriculture*, 46(1–3), 45–70. https://doi.org/10.1016/j.compag.2004.11.001
- Friedman, S. P., & Seaton, N. A. (1998). Critical path analysis of the relationship between permeability and electrical conductivity of three-dimensional pore networks. Water Resources Research, 34(7), 1703–1710. https://doi.org/10.1029/98wr00939
- Fu, Y., Horton, R., Ren, T., & Heitman, J. L. (2021). A general form of Archie's model for estimating bulk soil electrical conductivity. *Journal of Hydrology*, 597, 126160. https://doi.org/10.1016/j.jhydrol.2021.126160
- Fu, Y., Lu, Y., Heitman, J., & Ren, T. (2020). Root-induced changes in soil thermal and dielectric properties should not be ignored. *Geoderma*, 370, 114352. https://doi.org/10.1016/j.geoderma.2020.114352
- Fu, Y., Ren, T., Horton, R., & Heitman, J. L. (2023). Data for: An unsaturated hydraulic conductivity model based on the capillary bundle model, the Brooks-Corey model and Waxman-Smits model [Dataset]. HydroShare. Retrieved from http://www.hydroshare.org/ resource/0379b130021f45e3a011dd8772c234c3
- Fujimaki, H., & Inoue, M. (2003). A flux-controlled steady-state evaporation method for determining unsaturated hydraulic conductivity at low matric pressure head values. Soil Science, 168(6), 385–395. https://doi.org/10.1097/01.ss.0000075284.87447.cf
- Ghanbarian, B. (2020). Applications of critical path analysis to uniform grain packings with narrow conductance distributions: II. Water relative permeability. *Advances in Water Resources*, 137, 103524. https://doi.org/10.1016/j.advwatres.2020.103524
- Ghanbarian, B., Hunt, A. G., Ewing, R. P., & Sahimi, M. (2013). Tortuosity in porous media: A critical review. Soil Science Society of America Journal, 77(5), 1461–1477. https://doi.org/10.2136/sssaj2012.0435
- Ghanbarian, B., Ioannidis, M. A., & Hunt, A. G. (2017). Theoretical insight into the empirical tortuosity-connectivity factor in the Burdine-Brooks-Corey water relative permeability model. *Water Resources Research*, 53(12), 10395–10410. https://doi.org/10.1002/2017wr021753
- Ghanbarian, B., Torres-Verdín, C., & Skaggs, T. H. (2016). Quantifying tight-gas sandstone permeability via critical path analysis. *Advances in Water Resources*, 92, 316–322. https://doi.org/10.1016/j.advwatres.2016.04.015
- Ghanbarian, B., & Yokeley, B. A. (2021). Soil classification: A new approach for grouping soils using unsaturated hydraulic conductivity data. Water Resources Research, 57(9), e2021WR030095. https://doi.org/10.1029/2021wr030095
- Ghanbarian-Alavijeh, B., & Hunt, A. G. (2012). Unsaturated hydraulic conductivity in porous media: Percolation theory. *Geoderma*, 187, 77–84. https://doi.org/10.1016/j.geoderma.2012.04.007
- Gillham, R. W., Klute, A., & Heermann, D. F. (1979). Measurement and numerical simulation of hysteretic flow in a heterogeneous porous medium. Soil Science Society of America Journal, 43(6), 1061–1067. https://doi.org/10.2136/sssaj1979.03615995004300060001x
- Glover, P. (2009). What is the cementation exponent? A new interpretation. *The Leading Edge*, 28(1), 82–85. https://doi.org/10.1190/1.3064150 Gorman, T., & Kelly, W. E. (1990). Electrical-hydraulic properties of unsaturated Ottawa sands. *Journal of Hydrology*, 118(1–4), 1–18. https://doi.org/10.1016/0022-1694(90)90247-u

FU ET AL. 22 of 25

- Haverkamp, R., Bouraoui, F., Zammit, C., & Angulo-Jaramillo, R. (1998). Soil properties and moisture movement in the unsaturated zone. In J. Delleur (Ed.), *Handbook of groundwater engineering* (pp. 1–50). CRC Press.
- Haverkamp, R., Zammit, C., Boubkraoui, F., Rajkai, K., Arrue, J. L., & Heckmann, N. (1997). GRIZZLY, Grenoble soil catalogue: Soil survey of field data and description of particle-size, soil water retention and hydraulic conductivity functions. Laboratoire d'Etude des Transferts en Hydrologie et Environnement (LTHE).
- Hill (2004). Introduction to environmental soil physics. Elsevier.
- Iden, S. C., Peters, A., & Durner, W. (2015). Improving prediction of hydraulic conductivity by constraining capillary bundle models to a maximum pore size. *Advances in Water Resources*, 85, 86–92. https://doi.org/10.1016/j.advwatres.2015.09.005
- Ippisch, O., Vogel, H. J., & Bastian, P. (2006). Validity limits for the van Genuchten-Mualem model and implications for parameter estimation and numerical simulation. Advances in Water Resources, 29(12), 1780–1789. https://doi.org/10.1016/j.advwatres.2005.12.011
- Jackson, M. D. (2008). Characterization of multiphase electrokinetic coupling using a bundle of capillary tubes model. *Journal of Geophysical Research*, 113(B4), B04201. https://doi.org/10.1029/2007jb005490
- Johnson, D. L., Koplik, J., & Schwartz, L. M. (1986). New pore-size parameter characterizing transport in porous media. *Physical Review Letters*, 57(20), 2564–2567. https://doi.org/10.1103/physrevlett.57.2564
- Jury, W. A., & Horton, R. (2004). Soil physics (6th ed.). John Wiley.
- Katz, A. J., & Thompson, A. H. (1986). Quantitative prediction of permeability in porous rock. Physical Review B, 34(11), 8179–8181. https://doi.org/10.1103/physrevb.34.8179
- Kool, J. B., & Parker, J. C. (1987). Development and evaluation of closed-form expressions for hysteretic soil hydraulic properties. Water Resources Research, 23(1), 105–114. https://doi.org/10.1029/wr023i001p00105
- Kosugi, K. (1999). General model for unsaturated hydraulic conductivity for soils with Lognormal pore-size distribution. Soil Science Society of America Journal, 63(2), 270–277. https://doi.org/10.2136/sssaj1999.03615995006300020003x
- Lebeau, M., & Konrad, J. (2010). A new capillary and thin film flow model for predicting the hydraulic conductivity of unsaturated porous media. Water Resources Research, 46(12), 122457. https://doi.org/10.1029/2010wr009092
- Le Doussal, P. (1989). Permeability versus conductivity for porous media with wide distribution of pore sizes. *Physical Review B*, 39(7), 4816–4819. https://doi.org/10.1103/physrevb.39.4816
- Looy, K. V., Bouma, J., Herbst, M., Koestel, J., Minasny, B., Mishra, U., et al. (2017). Pedotransfer functions in Earth system science: Challenges and perspectives. *Reviews of Geophysics*, 55(4), 1199–1256. https://doi.org/10.1002/2017re000581
- Luckner, L., Genuchten, M. T. V., & Nielsen, D. R. (1989). A consistent set of parametric models for the two-phase flow of immiscible fluids in
- the subsurface. Water Resources Research, 25(10), 2187–2193. https://doi.org/10.1029/wr025i010p02187

 Martys, N., & Garboczi, E. J. (1992). Length scales relating the fluid permeability and electrical conductivity in random two-dimensional model
- porous media. *Physical Review B*, 46(10), 6080–6090. https://doi.org/10.1103/physrevb.46.6080

 Meerdink, J. S., Benson, C. H., & Khire, M. V. (1996). Unsaturated hydraulic conductivity of two compacted barrier soils. *Journal of Geotechni*-
- cal Engineering, 122(7), 565–576. https://doi.org/10.1061/(asce)0733-9410(1996)122:7(565)

 Mehta, B. K., Shiozawa, S., & Nakano, M. (1994). Hydraulic properties of a sandy soil at low water contents. Soil Science, 157(4), 208–214.
- https://doi.org/10.1097/00010694-199404000-00002
- Millington, R. J., & Quirk, J. P. (1961). Permeability of porous solids. Transactions of the Faraday Society, 57(0), 1200–1207. https://doi.org/10.1039/tf9615701200
- Minasny, B., & Field, D. J. (2005). Estimating soil hydraulic properties and their uncertainty: The use of stochastic simulation in the inverse modelling of the evaporation method. *Geoderma*, 126(3-4), 277-290. https://doi.org/10.1016/j.geoderma.2004.09.015
- Mualem, Y. (1976). A new model for predicting the hydraulic conductivity of unsaturated porous media. Water Resources Research, 12(3), 513–522. https://doi.org/10.1029/wr012i003p00513
- Mualem, Y. (1978). Hydraulic conductivity of unsaturated porous media: Generalized macroscopic approach. Water Resources Research, 14(2), 325–334. https://doi.org/10.1029/wr014i002p00325
- Mualem, Y., & Friedman, S. P. (1991). Theoretical prediction of electrical conductivity in saturated and unsaturated soil. *Water Resources Research*, 27(10), 2771–2777. https://doi.org/10.1029/91wr01095
- Nasta, P., Vrugt, J. A., & Romano, N. (2013). Prediction of the saturated hydraulic conductivity from Brooks and Corey's water retention parameters. Water Resources Research, 49(5), 2918–2925. https://doi.org/10.1002/wrcr.20269
- Nemes, A., Schaap, M. G., Leij, F. J., & Wösten, J. H. M. (2001). Description of the unsaturated soil hydraulic database UNSODA version 2.0. Journal of Hydrology, 251(3–4), 151–162. https://doi.org/10.1016/s0022-1694(01)00465-6
- Niu, Q., Fratta, D., & Wang, Y.-H. (2015). The use of electrical conductivity measurements in the prediction of hydraulic conductivity of unsaturated soils. *Journal of Hydrology*, 522, 475–487. https://doi.org/10.1016/j.jhydrol.2014.12.055
- NRCS. (1986). *Urban hydrology for small watersheds (No. 55)*. Engineering Division, Soil Conservation Service, US Department of Agriculture. O'Konski, C. T. (1960). Electric properties of macromolecules. V. Theory of ionic polarization in polyelectrolytes. *Journal of Physical Chemistry*, 64(5), 605–619. https://doi.org/10.1021/j100834a023
- Peters, A. (2013). Simple consistent models for water retention and hydraulic conductivity in the complete moisture range. Water Resources Research, 49(10), 6765–6780. https://doi.org/10.1002/wrcr.20548
- Peters, A., Hohenbrink, T. L., Iden, S. C., & Durner, W. (2021). A simple model to predict hydraulic conductivity in medium to dry soil from the water retention curve. Water Resources Research, 57(5), 1565. https://doi.org/10.1029/2020wr029211
- Pfannkuch, H. (1972). On the correlation of electrical conductivity properties of porous systems with viscous flow transport coefficients. *Developments in Soil Science*, 2, 42–54. https://doi.org/10.1016/s0166-2481(08)70527-0
- Purvance, D. T., & Andricevic, R. (2000). On the electrical-hydraulic conductivity correlation in aquifers. Water Resources Research, 36(10), 2905–2913. https://doi.org/10.1029/2000wr900165
- Reece, C. F. (1996). Evaluation of a line heat dissipation sensor for measuring soil matric potential. Soil Science Society of America Journal, 60(4), 1022–1028. https://doi.org/10.2136/sssaj1996.03615995006000040009x
- Revil, A., Ahmed, A. S., & Matthai, S. (2018). Transport of water and ions in partially water-saturated porous media. Part 3. Electrical conductivity. Advances in Water Resources, 121, 97–111. https://doi.org/10.1016/j.advwatres.2018.08.007
- Revil, A., Barnier, G., Karaoulis, M., Sava, P., Jardani, A., & Kulessa, B. (2014). Seismoelectric coupling in unsaturated porous media: Theory, petrophysics, and saturation front localization using an electroacoustic approach. *Geophysical Journal International*, 196(2), 867–884. https://doi.org/10.1093/gji/ggt440
- Revil, A., & Glover, P. W. J. (1998). Nature of surface electrical conductivity in natural sands, sandstones, and clays. Geophysical Research Letters, 25(5), 691–694. https://doi.org/10.1029/98g100296

FU ET AL. 23 of 25



- Rhoades, J. D., Raats, P. A. C., & Prather, R. J. (1976). Effects of liquid-phase electrical conductivity, water content, and surface conductivity on bulk soil electrical conductivity. Soil Science Society of America Journal, 40(5), 651–655. https://doi.org/10.2136/sssaj1976.03615995004000050017x
- Robinson, D. A., Campbell, C. S., Hopmans, J. W., Hornbuckle, B. K., Jones, S. B., Knight, R., et al. (2008). Soil moisture measurement for ecological and hydrological watershed-scale observatories: A review. *Vadose Zone Journal*, 7(1), 358–389. https://doi.org/10.2136/ vzi2007.0143
- Rudiyanto, Minasny, B., Chaney, N. W., Maggi, F., Giap, S. G. E., Shah, R. M., et al. (2021). Pedotransfer functions for estimating soil hydraulic properties from saturation to dryness. *Geoderma*, 403, 115194. https://doi.org/10.1016/j.geoderma.2021.115194
- Sakai, M., & Toride, N. (2007). Soil water hydraulic functions for a sandy soil and an aggregated soil [in Japanese with English abstract]. *Journal of the Japanese Society of Soil Physics*, 107, 63–77.
- Schaap, M., Condon, K., Durcik, M., & Losleben, M. (2021). CJCZO—Soil Moisture, soil temperature, electrical conductivity, water potential—Jemez 2013 Burned ZOB—(2010–2021) [Dataset]. HydroShare. Retrieved from http://www.hydroshare.org/resource/0348b65d71eb46d38bba7db4cb2826db
- Schaap, M. G., & Leij, F. J. (1998). Using neural networks to predict soil water retention and soil hydraulic conductivity. Soil and Tillage Research, 47(1–2), 37–42. https://doi.org/10.1016/s0167-1987(98)00070-1
- Schaap, M. G., & Leij, F. J. (2000). Improved prediction of unsaturated hydraulic conductivity with the Mualem-van Genuchten model. Soil Science Society of America Journal, 64(3), 843–851. https://doi.org/10.2136/sssaj2000.643843x
- Schaap, M. G., Leij, F. J., & van Genuchten, M. T. (2001). ROSETTA: A computer program for estimating soil hydraulic parameters with hierarchical pedotransfer functions. *Journal of Hydrology*, 251(3–4), 163–176. https://doi.org/10.1016/s0022-1694(01)00466-8
- Schindler, U., Durner, W., Unold, G., & Müller, L. (2010). Evaporation method for measuring unsaturated hydraulic properties of soils: Extending the measurement range. Soil Science Society of America Journal, 74(4), 1071–1083. https://doi.org/10.2136/sssaj2008.0358
- Schindler, U., & Müller, L. (2006). Simplifying the evaporation method for quantifying soil hydraulic properties. *Journal of Plant Nutrition and Soil Science*, 169(5), 623–629. https://doi.org/10.1002/jpln.200521895
- Schuh, W. M., & Cline, R. L. (1990). Effect of soil properties on unsaturated hydraulic conductivity pore-interaction factors. *Soil Science Society*
- of America Journal, 54(6), 1509–1519. https://doi.org/10.2136/sssaj1990.03615995005400060001x Skaggs, T. H. (2011). Assessment of critical path analyses of the relationship between permeability and electrical conductivity of pore networks.
- Skaggs, T. H. (2011). Assessment of critical path analyses of the relationship between permeability and electrical conductivity of pore network Advances in Water Resources, 34(10), 1335–1342. https://doi.org/10.1016/j.advwatres.2011.06.010
- Tindall, J. A., Kunkel, J. R., & Anderson, D. E. (1999). Unsaturated zone hydrology for scientists and engineers. Prentice Hall.
- Tokunaga, T. K. (2009). Hydraulic properties of adsorbed water films in unsaturated porous media. Water Resources Research, 45(6), W06415. https://doi.org/10.1029/2009wr007734
- Topp, G. C. (1969). Soil-water hysteresis measured in a sandy loam and compared with the hysteretic domain model. Soil Science Society of America Journal, 33(5), 645–651. https://doi.org/10.2136/sssaj1969.03615995003300050011x
- Topp, G. C. (1971). Soil water hysteresis in silt loam and clay loam soils. Water Resources Research, 7(4), 914–920. https://doi.org/10.1029/wr007i004p00914
- Tuli, A., & Hopmans, J. W. (2004). Effect of degree of fluid saturation on transport coefficients in disturbed soils. European Journal of Soil Science, 55(1), 147–164. https://doi.org/10.1046/j.1365-2389.2002.00493.x-i1
- Tuller, M., & Or, D. (2001). Hydraulic conductivity of variably saturated porous media: Film and corner flow in angular pore space. Water Resources Research, 37(5), 1257–1276. https://doi.org/10.1029/2000wr900328
- Twarakavi, N. K. C., Šimůnek, J., & Schaap, M. G. (2010). Can texture-based classification optimally classify soils with respect to soil hydraulics? Water Resources Research, 46(1), e0131299. https://doi.org/10.1029/2009wr007939
- van Dam, J. C., Stricker, J. N. M., & Droogers, P. (1994). Inverse method to determine soil hydraulic functions from multistep outflow experiments. Soil Science Society of America Journal, 58(3), 647–652. https://doi.org/10.2136/sssaj1994.03615995005800030002x
- van Genuchten, M. T. (1980). A closed-form equation for predicting the hydraulic conductivity of unsaturated soils. Soil Science Society of America Journal, 44(5), 892–898. https://doi.org/10.2136/sssaj1980.03615995004400050002x
- van Lier, Q. J., & Pinheiro, E. A. R. (2018). An alert regarding a common misinterpretation of the van Genuchten α parameter. Revista Brasileira de Ciência do Solo, 42, e0170343. https://doi.org/10.1590/18069657rbcs20170343
- Vereecken, H. (1995). Estimating the unsaturated hydraulic conductivity from theoretical models using simple soil properties. *Geoderma*, 65(1–2), 81–92. https://doi.org/10.1016/0016-7061(95)92543-x
- Vereecken, H., Maes, J., & Feyen, J. (1990). Estimating unsaturated hydraulic conductivity from easily measured soil properties. *Soil Science*, 149(1), 1–12. https://doi.org/10.1097/00010694-199001000-00001
- Vereecken, H., Weynants, M., Javaux, M., Pachepsky, Y., Schaap, M. G., & van Genuchten, M. T. (2010). Using pedotransfer functions to estimate the van Genuchten–Mualem soil hydraulic properties: A review. Vadose Zone Journal, 9(4), 795–820. https://doi.org/10.2136/vzj2010.0045
- Vogel, T., Genuchten, M. T. V., & Cislerova, M. (2000). Effect of the shape of the soil hydraulic functions near saturation on variably-saturated flow predictions. Advances in Water Resources, 24(2), 133–144. https://doi.org/10.1016/s0309-1708(00)00037-3
- Wang, Y., Ma, R., & Zhu, G. (2022). Improved prediction of hydraulic conductivity with a soil water retention curve that accounts for both capillary and adsorption forces. *Water Resources Research*, 58(4), e2021WR031297. https://doi.org/10.1029/2021wr031297
- Waxman, M. H., & Smits, L. J. M. (1968). Electrical conductivities in oil-bearing shaly sands. Society of Petroleum Engineers Journal, 8(02), 107–122. https://doi.org/10.2118/1863-a
- Weber, T. K. D., Finkel, M., Gonçalves, M., Vereecken, H., & Diamantopoulos, E. (2020). Pedotransfer function for the Brunswick soil hydraulic property model and comparison to the van Genuchten-Mualem model. *Water Resources Research*, 56(9), e2019WR026820. https://doi.org/10.1029/2019wr026820
- Weynants, M., Montanarella, L., Tóth, G., Arnoldussen, A., Anaya Romero, M., Bilas, G., et al. (2013). European HYdropedological data Inventory (EU-HYDI), EUR—Scientific and technical research series (pp. 1831–9424).
- Weynants, M., Vereecken, H., & Javaux, M. (2009). Revisiting Vereecken pedotransfer functions: Introducing a closed-form hydraulic model. Vadose Zone Journal, 8(1), 86–95. https://doi.org/10.2136/vzj2008.0062
- Wildenschild, D., Hopmans, J. W., & Simunek, J. (2001). Flow rate dependence of soil hydraulic characteristics. *Soil Science Society of America Journal*, 65(1), 35–48. https://doi.org/10.2136/sssai2001.65135x
- Wildenschild, D., Jensen, K. H., Hollenbeck, K. J., Sonnenborg, T., Butts, M. B., Illangasekare, T. H., & Znidarcic, D. (1997). A two-stage procedure for determining unsaturated hydraulic characteristics using a syringe pump and outflow observations. Soil Science Society of America Journal, 61(2), 347–359. https://doi.org/10.2136/sssaj1997.03615995006100020002x
- Wösten, J. H. M., Lilly, A., Nemes, A., & Bas, C. L. (1999). Development and use of a database of hydraulic properties of European soils. *Geoderma*, 90(3–4), 169–185. https://doi.org/10.1016/s0016-7061(98)00132-3

FU ET AL. 24 of 25

- Yates, S. R., Genuchten, M. T., Warrick, A. W., & Leij, F. J. (1992). Analysis of measured, predicted, and estimated hydraulic conductivity using the RETC computer program. Soil Science Society of America Journal, 56(2), 347–354. https://doi.org/10.2136/sssaj1992.03615995005600020003x
- Zhang, M., Lu, Y., Heitman, J., Horton, R., & Ren, T. (2017). Temporal changes of soil water retention behavior as affected by wetting and drying following tillage. Soil Science Society of America Journal, 81(6), 1288–1295. https://doi.org/10.2136/sssaj2017.01.0038
- Zhang, X., & Knackstedt, M. A. (1995). Direct simulation of electrical and hydraulic tortuosity in porous solids. *Geophysical Research Letters*, 22(17), 2333–2336. https://doi.org/10.1029/95g102230
- Zhang, Y., & Schaap, M. G. (2017). Weighted recalibration of the Rosetta pedotransfer model with improved estimates of hydraulic parameter distributions and summary statistics (Rosetta3). *Journal of Hydrology*, 547, 39–53. https://doi.org/10.1016/j.jhydrol.2017.01.004
- Zhang, Z. F. (2011). Soil water retention and relative permeability for conditions from oven-dry to full saturation. *Vadose Zone Journal*, 10(4), 1299–1308. https://doi.org/10.2136/vzj2011.0019

FU ET AL. 25 of 25